Stem Cell Reports
Article

ISSCR

OPEN ACCESS

Functional redundancy among Polycomb complexes in maintaining the pluripotent state of embryonic stem cells

Yaru Zhu,[1,5] Lixia Dong,[1,5] Congcong Wang,[1,5] Kunying Hao,[1,5] Jingnan Wang,[1] Linchun Zhao,[1] Lijun Xu,[1] Yin Xia,[2] Qing Jiang,[3] and Jinzhong Qin[1,4,*]

[1]State Key Laboratory of Pharmaceutical Biotechnology and MOE Key Laboratory of Model Animals for Disease Study, Model Animal Research Center, Medical School of Nanjing University, 12 Xuefu Road, Nanjing, Jiangsu 210061, China
[2]School of Biomedical Sciences, The Chinese University of Hong Kong, Hong Kong, China
[3]Department of Sports Medicine and Adult Reconstructive Surgery, Nanjing Drum Tower Hospital Affiliated to Medical School of Nanjing University, Nanjing, China
[4]Jiangsu Key Laboratory of Molecular Medicine, Medical School of Nanjing University, Nanjing 210093, China
[5]These authors contributed equally
*Correspondence: qinjz@nju.edu.cn
https://doi.org/10.1016/j.stemcr.2022.02.020

SUMMARY

Polycomb group proteins assemble into multi-protein complexes, known as Polycomb repressive complexes 1 and 2 (PRC1 and PRC2), that guide cell fate decisions during embryonic development. PRC1 forms an array of biochemically distinct canonical PRC1 (cPRC1) or non-canonical PRC1 (ncPRC1) complexes characterized by the mutually exclusive presence of PCGF (PCGF1-PCGF6) paralog subunit; however, whether each one of these subcomplexes fulfills a distinct role remains largely controversial. Here, by performing a CRISPR-based loss-of-function screen in embryonic stem cells (ESCs), we uncovered a previously unappreciated functional redundancy among PRC1 subcomplexes. Disruption of ncPRC1, but not cPRC1, displayed severe defects in ESC pluripotency. Remarkably, coablation of non-canonical and canonical PRC1 in ESCs resulted in exacerbation of the phenotype observed in the non-canonical PRC1-null ESCs, highlighting the importance of functional redundancy among PRC1 subcomplexes. Together, our studies demonstrate that PRC1 subcomplexes act redundantly to silence lineage-specific genes and ensure robust maintenance of ESC identity.

INTRODUCTION

Embryonic stem cells (ESCs), derived from the inner cell mass (ICM), have an extraordinary self-renewal capacity and yet retain pluripotency, which is the ability of cells to differentiate into any cell type of the three germ layers (Evans and Kaufman, 1981; Martin, 1981). A considerable body of work carried out over the past four decades has led to the view that the ESC state is transcriptionally controlled by OCT4, SOX2, and NANOG with chromatin regulators (Boyer et al., 2005). The Polycomb group (PcG) proteins are a set of evolutionary conserved factors that form chromatin regulator complexes involved in the transcriptional repression of key developmental genes to preserve cell fates (Piunti and Shilatifard, 2021; Schuettengruber et al., 2017; Simon and Kingston, 2009). PcG proteins assemble into two major chromatin-modifying multi-protein complexes, Polycomb repressive complexes 1 and 2 (PRC1 and PRC2). PRC2 is composed of four core components SUZ12, EED, RBAP46/48, and the histone methyltransferases EZH1/2, which mono-, di-, and trimethylate lysine 27 of histone H3 (H3K27me1/2/3) (Piunti and Shilatifard, 2021). In addition, several sub-stoichiometric PRC2 accessory components have been identified, including JARID2, AEBP2, and PCL1-3, which modulate the recruitment to chromatin and/or enzymatic activity of the PRC2 complex.

Drosophila PRC1 contains Polycomb (Pc), Sex Combs Extra (Sce/dRing), Posterior Sex Combs (Psc), Polyhomeotic (Ph), and a sub-stoichiometric amount of Sex Comb on Midleg (Scm) (Saurin et al., 2001). Each of these proteins has multiple orthologs in mammals classified, respectively, as the CBX, RING1A/B, PCGF, PHC, and SCMH1/SCML2 families (Simon and Kingston, 2009). Mammalian PRC1 complexes are more heterogeneous in composition than PRC2 since each of the Drosophila core subunits has several orthologs that can interact in a combinatorial fashion. The ubiquitin E3 ligase RING1A/B, which monoubiquitylates histone 2A on lysine 119 (H2AK119ub1), can interact with one of six mutually exclusive PCGF paralog subunits (PCGF1-PCGF6), thereby creating six biochemically distinct PRC1 subcomplexes (named PRC1.1-PRC1.6) with diverse subunit composition whose functions are largely unknown (Gao et al., 2012). In addition to the core subunits, all PRC1 complexes incorporate versatile accessory proteins that confer functional specificity to a given complex. Importantly, these subcomplexes can be further divided into canonical (cPRC1) or non-canonical (ncPRC1), with cPRC1-containing PCGF2 or PCGF4, one of the PHC (PHC1/2/3), SCMH1/SCML2, and one of the CBX (CBX2/4/6/7/8) proteins that recognizes the H3K27me3 mark deposited by PRC2 (Gao et al., 2012; Piunti and Shilatifard, 2021; Schuettengruber et al.,

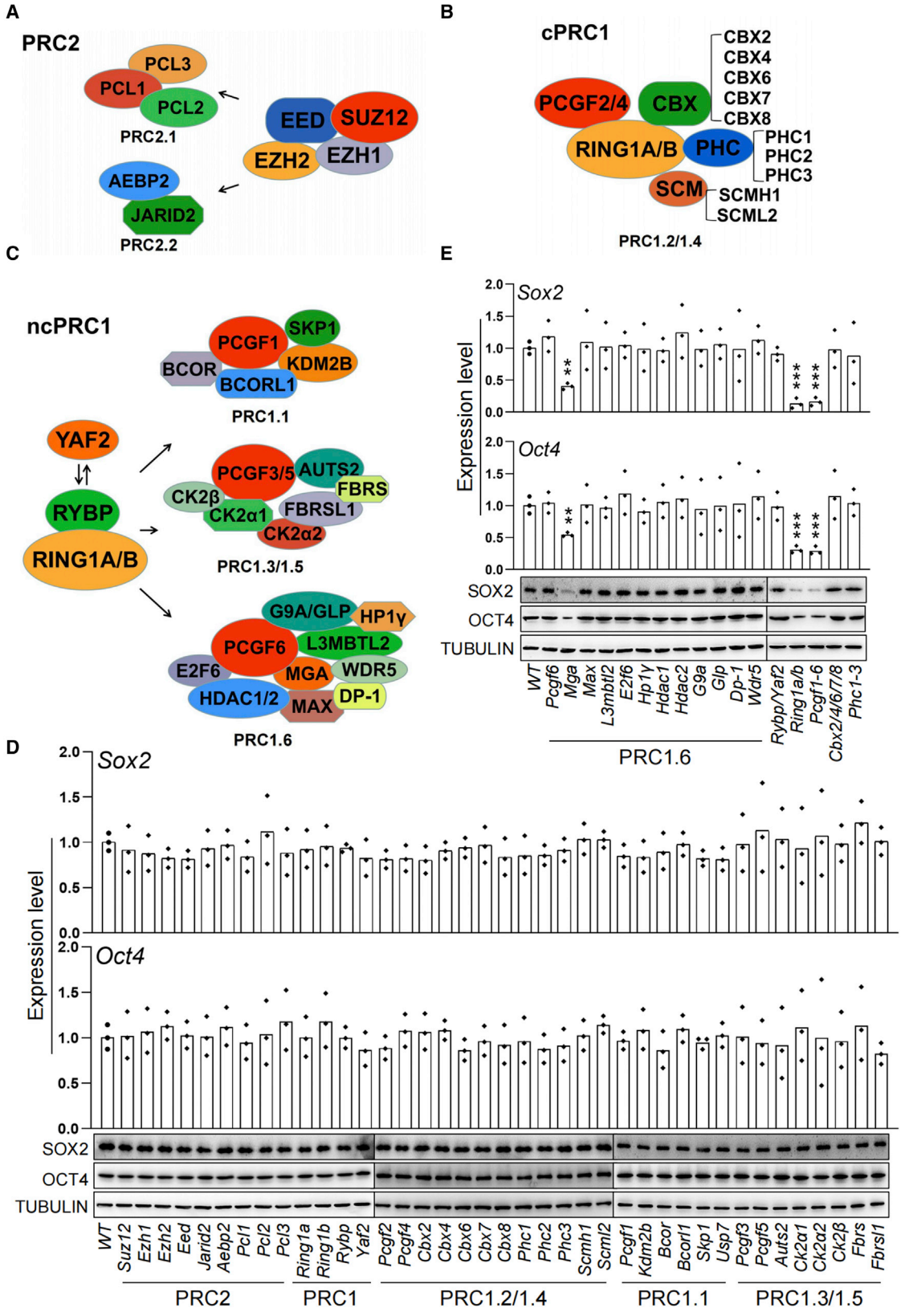

(legend on next page)

2017). Conversely, ncPRC1 contain RYBP or YAF2 instead of CBX and PHC subunits, one of the four PCGF proteins (PCGF1/3/5/6), and therefore are targeted to chromatin independently of H3K27me3.

Although the molecular compositions of distinct PRC1 family complexes have been determined, their diverse biological functions and the crosstalk among the different complexes remain to be fully elucidated. While complete loss of PRC1 in mice via ablation of *Ring1a/b* results in pre-implantation lethality at the two-cell stage (Posfai et al., 2012), loss-of-function studies of *Pcgfs* in mice highlight major but distinct roles for the different PRC1 complexes in development (Akasaka et al., 2001; Almeida et al., 2017; Dickinson et al., 2016; Endoh et al., 2017; Liu et al., 2020). Obviously, ablation of individual PCGF proteins independently does not reproduce the loss of RING1A/B activity, suggesting that distinct PRC1 complexes may cooperate to determine *Ring1a/b* biological functions. Here, we utilize the CRISPR-Cas9 system to create single or combined *Pcgf* knockout in ESCs and rigorously investigate their functions in maintaining ESC pluripotency. We demonstrate that simultaneous, but not individual, ablation of *Pcgfs* led to loss of pluripotency in ESCs and triggers impaired self-renewal and spontaneous differentiation, a phenotype reminiscent of those in *Ring1a/b* double-deficient ESCs. Collectively, our data provide evidence that distinct PRC1 family complexes share a redundant but essential role in the maintenance of the pluripotent state in ESCs.

RESULTS

CRISPR screen in ESCs reveals the potential involvement of the *Pcgf* family in the maintenance of pluripotency

To explore the molecular mechanisms governing ESC pluripotency, we first screened for components in the PcG family (Figures 1A–1C), whose deficiency resulted in the changes of ESC identity genes *Oct4* (also known as *Pou5f1*), and *Sox2*. We deleted individual PcG genes via a dual sgRNA-directed CRISPR-Cas9 system in ESCs and then evaluated the expression of *Oct4* and *Sox2* by qRT-PCR and western blot (Qin et al., 2021) (Figures 1D and 1E). We found that CRISPR-Cas9-mediated knockout of *Mga*, but not those of other PcG family members, was accompanied by a significant reduction in the expression of *Oct4* and *Sox2*, which is consistent with our previous findings (Qin et al., 2021). In mammals, each of the PRC1 core subunits has two or more homologs (Figures 1B and 1C). We reasoned that the absence of a loss-of-function phenotype for PcG core subunits is due to compensation by their closely related homologs. To this end, we generated *Rybp/Yaf2* or *Ring1a/b* double, *Phc1/2/3* triple, *Cbx2/4/6/7/8* quintuple and *Pcgf1-6* sextuple knockout ESCs. We found that knockout of all six *Pcgfs* or *Ring1a/b* led to dramatic reduction in the expression levels of *Oct4* and *Sox2* (Figure 1E), whereas the loss of five *Cbxs*, three *Phcs*, or *Rybp/Yaf2* has no detectable effect (see below for more details). Interestingly, E3 ubiquitin ligases RING1A/B are responsible for the maintenance of H2AK119ub1 when paired with one of six PCGF partners. In this study, we decided to further investigate the potential role of PCGF family in maintaining ESC pluripotency.

Loss of individual PCGF family members has no significant effect on the maintenance of ESC identity

To rigorously explore the role of PCGF family in ESCs, we first determined whether these *Pcgfs* are expressed in ESCs. As assessed by western blot analysis, each PCGF family member is expressed in ESCs (Figure 2A). We generated cohorts of ESCs deficient in individual *Pcgfs* (Figures S1A–S1F). The loss of PCGF protein expression was confirmed by western blot analysis (Figure 2A). Single knockout of *Pcgfs* did not appear to appreciably affect histone modifications (H2AK119ub1 and H3K27me3) and protein levels of other PcG family members we examined (Figures 2A and 2B). These mutant cells were monitored for their capacity to form colonies after seeding on mitotically inactivated mouse embryonic fibroblast feeder layer. Consistent with our previous reports (Yan et al., 2017; Zhao et al., 2017a, 2017b), the single *Pcgf-null* ESCs were viable and retained a typical undifferentiated state as characterized by colony morphology, staining for alkaline phosphatase (AP), expression of the pluripotency-associated transcription factors, namely *Nanog*, *Sox2*, and *Oct4*, even after long-term culture (Figures 2B and 2C). Notably, loss of *Pcgf6* gave rise to colonies that were smaller in size, whereas the targeted inactivation of other *Pcgfs* had no significant effect on overall cell growth. The teratoma formation in recipient mice is often considered as gold standard for pluripotency testing of ESCs. After 4–6 weeks of subcutaneous injection of mutant ESCs into nude mice, teratomas containing

Figure 1. Effect of ablation of PcG genes on the expression of core pluripotency transcription factors *Oct4* and *Sox2* in ESCs

(A–C) (A) Schematic representation of the subunit composition of the mammalian PRC2, (B) cPRC1, and (C) ncPRC1 complexes.

(D and E) Effect of CRISPR-mediated knockout of PcG genes on the expression of the pluripotency core regulators *Oct4* and *Sox2* in ESCs determined by qRT-PCR (top) and western blot (bottom). Each value was normalized to its corresponding actin value and the expression level in wild-type (WT) ESCs was arbitrarily set to 1. Data in (D) and (E) represent mean ± SD obtained from three independent experiments, $^{*}p < 0.05$, $^{**}p < 0.01$, $^{***}p < 0.001$ (Student's t test) compared with the control.

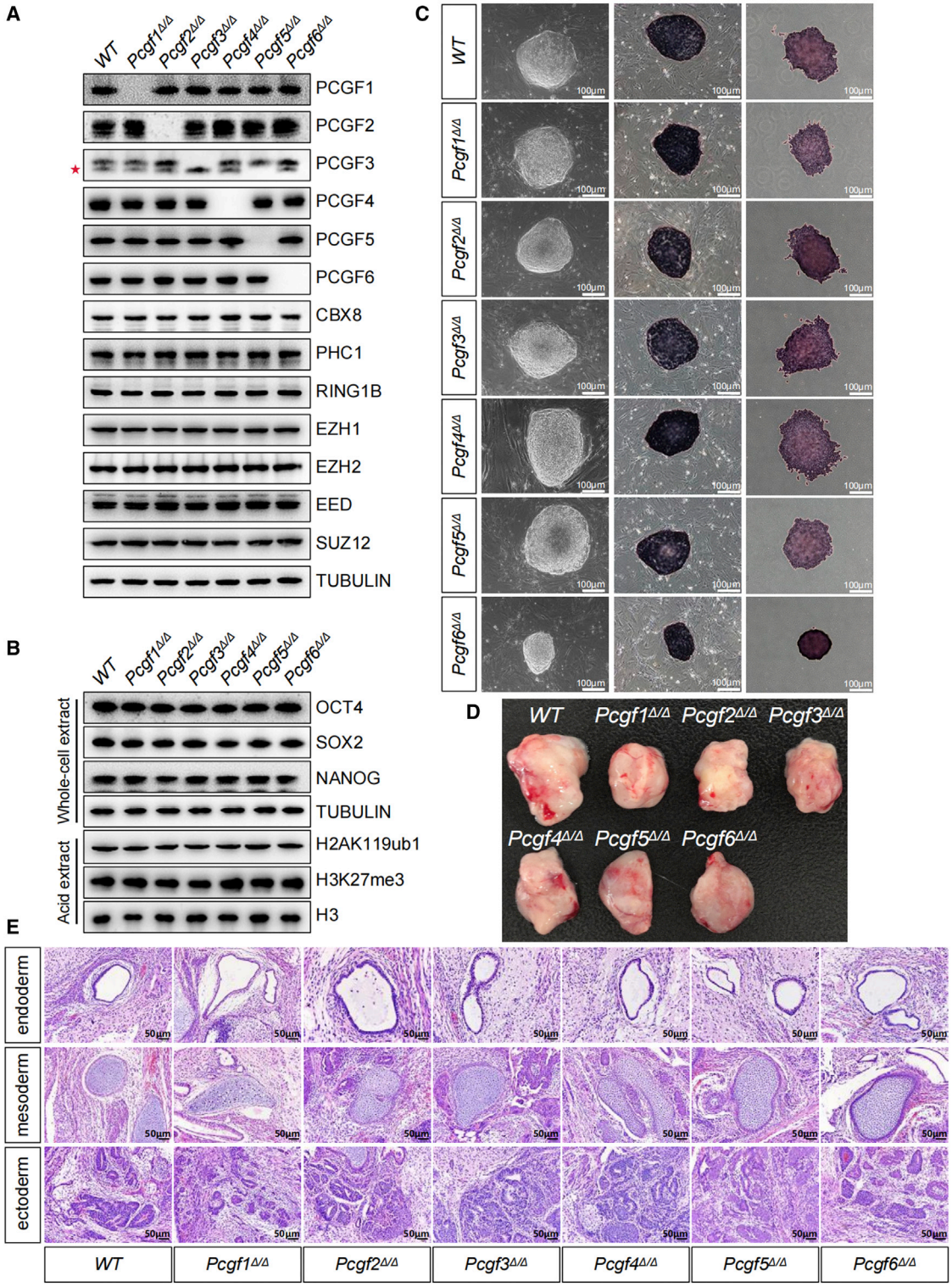

Figure 2. Loss of individual PCGF family members has no or a mild effect on the pluripotent properties of ESCs

(A) Western blot analyses showing changes in the global levels of PcG proteins in ESCs of indicated genotypes. Note, the PCGF3 antibody also recognized PCGF5 (*).

(legend continued on next page)

derivatives of all three embryonic germ layers were observed, indicating that these cells maintained pluripotency (Figures 2D and 2E). No or a very mild phenotype in single mutants can likely be attributed to functional redundancy among the *Pcgf* members.

RING1A/B play essential and redundant roles in ESC pluripotency maintenance

RING1A/B are subunits shared by all major PRC1 complexes (Figures 1B and 1C). Therefore, we set out to characterize the functions of RING1A/B in ESCs by generating ESCs deficient in *Ring1a* (*Ring1a*$^{\Delta/\Delta}$) or *Ring1b* (*Ring1b*$^{\Delta/\Delta}$) (Figures S1G and S1H). Interestingly, disruption of Ring1b led to increased RING1A protein levels, and vice versa (Figure 3A), suggesting that the loss of one can be compensated by upregulation of the other. In addition, ablation of *Ring1b* in ESCs caused complete loss of PCGF2 and dramatic upregulation of PCGF4. *Ring1a*$^{\Delta/\Delta}$ or *Ring1b*$^{\Delta/\Delta}$ cells did not show any noticeable phenotype and proliferated normally in the undifferentiated state (Figures 3B and 3C). Teratoma studies revealed that, while *Ring1a*$^{\Delta/\Delta}$ cells produced teratomas containing all three germ layer lineages, *Ring1b*$^{\Delta/\Delta}$ cells developed teratomas containing structures pertaining to all three germ layers but with an overrepresentation of the endoderm structures (Figure S2A).

To examine possible functional redundancy between RING1A and RING1B in ESCs, we established *Ring1a*$^{\Delta/\Delta}$;*Ring1b*$^{F/F}$ ESC lines (Figure S1H), in which *Ring1b* could be conditionally ablated by transient expression of Cre recombinase. RING1B was completely removed 72 h after Cre transfection (Figure S2B), and loss of *Ring1b* resulted in no detectable H2AK119ub1, which was largely unaffected in any of the single mutants (Figure 3B). Therefore, throughout this study, unless otherwise stated, the cells were used for assay after 72 h of Cre transfection. Remarkably, in contrast to each single knockout, *Ring1a/b* double-deficient ESCs exhibited severely impaired self-renewal capacity, suggesting their redundant role in ESC pluripotency maintenance. Combined deletion of *Ring1a/b* led to massive cell death by apoptosis (23.3% Annexin V binding in *Ring1a/b*$^{\Delta/\Delta}$ cells versus 15.1% in control *Ring1a*$^{\Delta/\Delta}$;*Ring1b*$^{F/F}$ cells), whereas both single mutants displayed the same apoptotic rates as the wild type. Cell-cycle analysis revealed that *Ring1a/b* double, but not single mutants exhibited a markedly extended G1 phase and a shortened S phase, suggesting that the impaired growth of *Ring1a/b*$^{\Delta/\Delta}$ ESCs was due to combinatory effect of cell-cycle perturbation and apoptosis induction (Figures S2C and S2D). Double ablation of *Ring1a/b* resulted in the formation of flat and morphologically distinct colonies and in a significant decrease of AP staining indicative of precocious differentiation (Figure 3C). *Ring1a/b*$^{\Delta/\Delta}$ ESCs could not be propagated beyond six passages when cultured under conditions that favor ESC maintenance, indicating an essential role for maintaining ESC identity. As cell passages increased, *Ring1a/b*$^{\Delta/\Delta}$ ESCs gradually lost their proliferation potential, as indicated by an increased proportion of cells in G1 phase and a decreased proportion of cells in S phase (Figure S2E). Because the loss of *Ring1a/b* in ESCs was accompanied by declines in *Nanog*, *Sox2*, and *Oct4* mRNA and protein levels (Figure 3B; Tables S1–S3), we investigated whether RING1A/B contributed to the maintenance of stem cell identity through regulation of these core pluripotency factors. The *Ring1a/b-null* rescue system utilized *Ring1a*$^{\Delta/\Delta}$;*Ring1b*$^{F/F}$ ESCs, in which the floxed *Ring1b* alleles were excised by Cre recombinase. Introducing *Oct4*, *Nanog*, or *Sox2* using lentivirus-mediated transduction did not significantly restore the defects observed in *Ring1a/b*$^{\Delta/\Delta}$ ESCs (Figures S2F and S2G). In contrast, the range of phenotypes observed in the *Ring1a/b*$^{\Delta/\Delta}$ ESCs were rescued by the ectopic expression of either *Ring1a* or *Ring1b* (Figures 3C–3E). Thus, the function of RING1A/B in maintaining ESC identity appears not to be mediated by keeping the requisite levels of OCT4, NANOG, and SOX2. In addition, although *Ring1a*$^{\Delta/\Delta}$ or *Ring1b*$^{\Delta/\Delta}$ retained the ability to form teratomas, the capability of producing teratomas was completely abolished in *Ring1a/b* double knockout ESCs (Figure S2H), supporting the functional redundancy of RING1A and RING1B. Thus, RING1A/B play redundant but collectively essential roles in the maintenance of stem cell identity.

To gain insight into the molecular mechanisms underlying the observed phenotypic changes, we performed RNA-seq analysis in single and double *Ring1a/b* knockout ESCs (Tables S1–S3). Complete loss of *Ring1a/b* in ESCs resulted in substantial changes in gene expression (3,714 upregulated versus 1,541 downregulated genes) (Figures 3F and

(B) Western blot analyses showing changes in the global levels of pluripotency factors, H2AK119ub1 and H3K27me3 in ESCs of indicated genotypes. Tubulin and H3 were used as loading controls.

(C) Left: phase-contrast images of ESC colonies cultured on a feeder layer of MEFs. Middle and right: representative images of AP staining of WT and mutant ESC colonies cultured on a feeder layer of MEFs (middle) or gelatin (right). Scale bar, 100 μm.

(D) Teratoma formation in immunodeficiency mice by ESCs of indicated genotypes.

(E) Representative images of tissues of all three germ layers, including gut epithelium (endoderm), cartilage (mesoderm), and neural rosette (ectoderm), from H&E staining of teratomas generated from ESCs of the indicated genotypes. Shown is a representative of three injected mice. Scale bars, 50 μm.

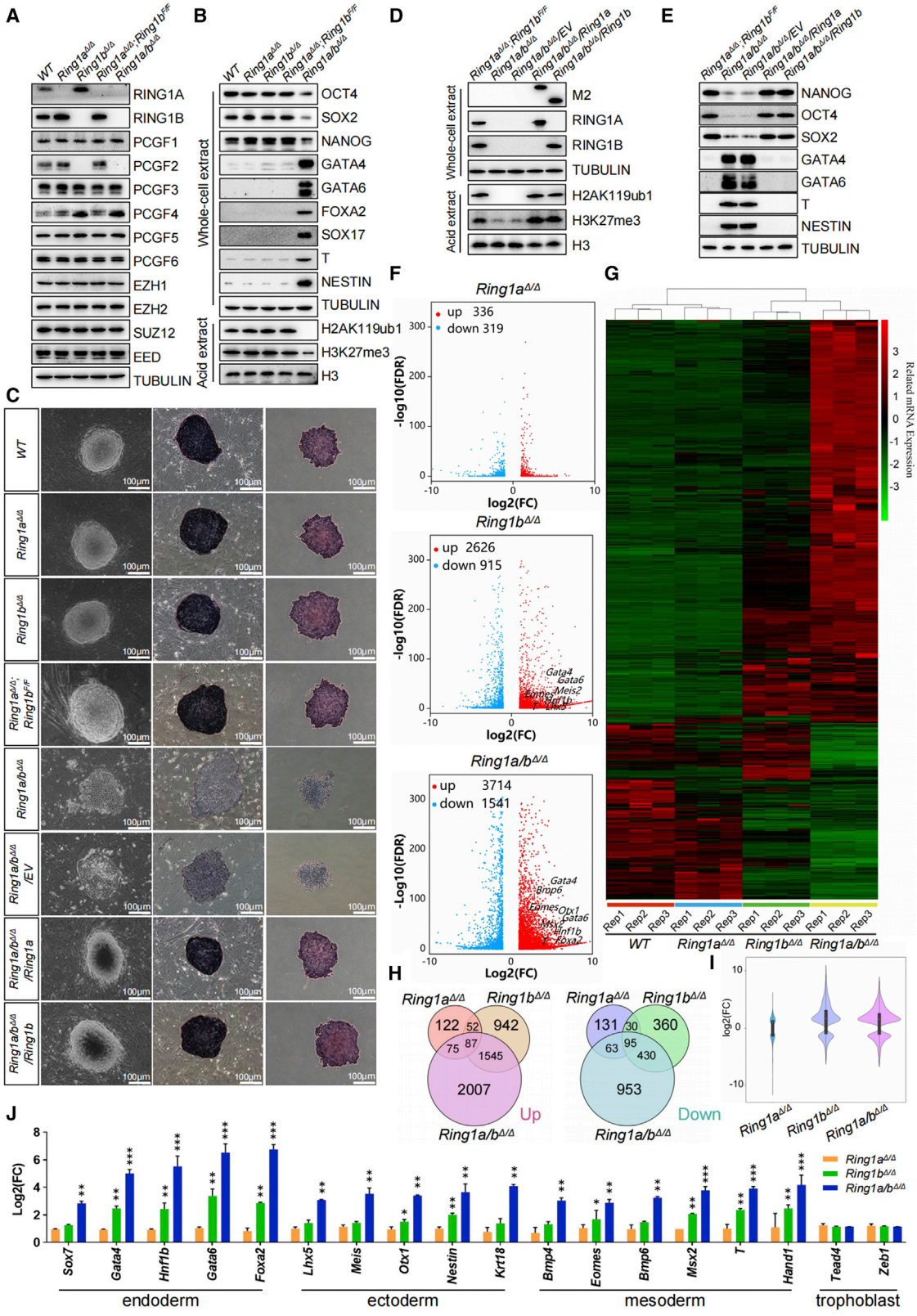

(legend on next page)

3G; Table S3). More genes were upregulated than downregulated upon loss of *Ring1a/b*, consistent with their essential role in transcriptional gene silencing. In contrast, only 655 (336 up, and 319 down) and 3,541 (2,626 up, and 915 down) genes were deregulated in *Ring1a* and *Ring1b* single mutants, respectively, further supporting the existence of functional redundancy between RING1A and RING1B (Tables S1–S3). The genes that were altered in $Ring1a^{\Delta/\Delta}$ and $Ring1b^{\Delta/\Delta}$ ESCs highly correlated and overlapped with those altered in *Ring1a/b* double null ESCs (Figures 3H and 3I). Gene ontology (GO) analysis on differentially expressed genes in *Ring1a/b-null* ESCs showed that upregulated genes are primarily linked to developmental processes, including pattern specification process, cell fate commitment and organ morphogenesis. In contrast, downregulated genes were specifically enriched for genes associated with mechanisms associated with pluripotency and chemotaxis, consistent with the observed proliferation defects (Figures S2I and S2J). Importantly, examination of upregulated genes in $Ring1a/b^{\Delta/\Delta}$ ESCs also showed a notable overrepresentation of germ layer lineage-specific transcripts, including master regulators of endoderm formation (such as *Sox7*, *Gata4*, *Hnf1b*, *Gata6*, and *Foxa2*) (Figure 3J), key markers of ectoderm (*Meis*, *Lhx5*, *Otx1*, *Nestin*, and *Krt18*) or mesoderm (such as *Bmp4*, *Eomes*, *Bmp6*, *Msx2*, *T*, and *Hand1*). In contrast, expression levels of key markers of trophectoderm (*Tead4* and *Zeb1*), either decreased or remained the same in mutant cells (Table S3). By performing qRT-PCR, western blot analysis and immunofluorescence (IF), we confirmed the RNA-seq finding and demonstrated that, while the expression of these genes was significantly upregulated in $Ring1a/b^{\Delta/\Delta}$ ESCs, their expression was largely unaffected or moderately increased in $Ring1a^{\Delta/\Delta}$ and $Ring1b^{\Delta/\Delta}$ ESCs, respectively (Figures 3B, 3J, and S3). Together, these data suggest that RING1A/B act redundantly to repress lineage-specific developmental genes and safeguard self-renewal and pluripotency in ESCs.

PCGF2/4 is dispensable for both the maintenance and differentiation of the ESCs

The cPRC1 complexes assemble around the RING1A/B-PCGF2/4 core and contain one of the CBX2/4/6/7/8 subunits and one of the PHC1/2/3 proteins (Schuettengruber et al., 2017; Shao et al., 1999) (Figure 1B). To overcome possible functional redundancy and compensation of the canonical PCGF family members, *Pcgf2/4* double knockout ESC lines ($Pcgf2/4^{\Delta/\Delta}$) were established. These cells maintained compact dome-shaped colony morphology similar to that of the wild-type ESCs (Figure 4A). Combined deletions of *Pcgf2/4* did not appreciably affect the expression levels of the remaining PcG family members (Figure 4B). They also expressed high levels of the pluripotency markers AP, OCT4, NANOG, and SOX2 without any signs of differentiation into three germ lineages (Figures 4A and 4C). In addition, $Pcgf2/4^{\Delta/\Delta}$ ESCs exhibited high replating efficiency and they maintain their ability to differentiate into representative tissues of the three embryonic germ layers (Figure 4D). In addition, to explore directly the potential role for CBX2/4/6/7/8 and PHC1/2/3 in maintaining the pluripotency of ESCs, we generated triple and quintuple mutants of the *Phc1/2/3* ($Phc1/2/3^{\Delta/\Delta}$) and *Cbx2/4/6/7/8* ($Cbx2/4/6/7/8^{\Delta/\Delta}$) subfamilies, respectively (Figures S4A–S4H). Surprisingly, both mutants, similar to $Pcgf2/4^{\Delta/\Delta}$ ESCs, possessed the ability to self-renew in an undifferentiated state under standard culture conditions while retaining

Figure 3. RING1A/B coordinate redundant mechanisms that ensure robust repression of key lineage-specific genes for sustaining ESC identity

(A and B) (A) Western blot demonstrating changes in the levels of PcG proteins, (B) pluripotency factors, endodermal (GATA4, GATA6, FOXA2, SOX17), mesodermal (T), and ectodermal (NESTIN) markers in ESCs of indicated genotypes. Tubulin and H3 were used as loading controls.

(C) Left: phase-contrast images of ESC colonies of indicated genotypes cultured on a feeder layer of MEFs. Middle and right: images of ESC colonies cultured on feeder layers (middle) or gelatin (right) after AP staining. Scale bar, 100 μm.

(D and E) (D) Western blot for selected PcG proteins, H2AK119ub1, H3K27me3, (E) pluripotency factors and selected germ layer markers in ESCs of indicated genotypes. The expression levels of the indicated FLAG-tagged proteins were detected with anti-Flag M2 antibody. Tubulin and H3 were used as loading controls.

(F) Volcano plots of −log10 (p value) against log2-fold change representing the differences in gene expression in ESCs of indicated genotypes. Upregulated (red) and downregulated (blue) genes are highlighted.

(G) Heatmap depicting fold changes in gene expression in ESCs of indicated genotypes. False discovery rate <0.05. Up- and downregulated genes are reported as red and green, respectively.

(H) Venn diagram showing overlap of upregulated (top) or downregulated (bottom) genes in $Ring1a^{\Delta/\Delta}$, $Ring1b^{\Delta/\Delta}$, and $Ring1a/b^{\Delta/\Delta}$ ESCs.

(I) A violin plot comparing log2-fold changes of genes in ESCs deficient for *Ring1a*, *Ring1b*, or both.

(J) qRT-PCR analysis of changes in the expression of lineage-specific genes. Each value was normalized to actin expression, and for each gene, the expression level in the wild-type ESCs was arbitrarily set to 1. Data are shown as the means ± SD for triplicate analysis. *$p < 0.05$, **$p < 0.01$, ***$p < 0.001$ (Student's t test) compared with the control.

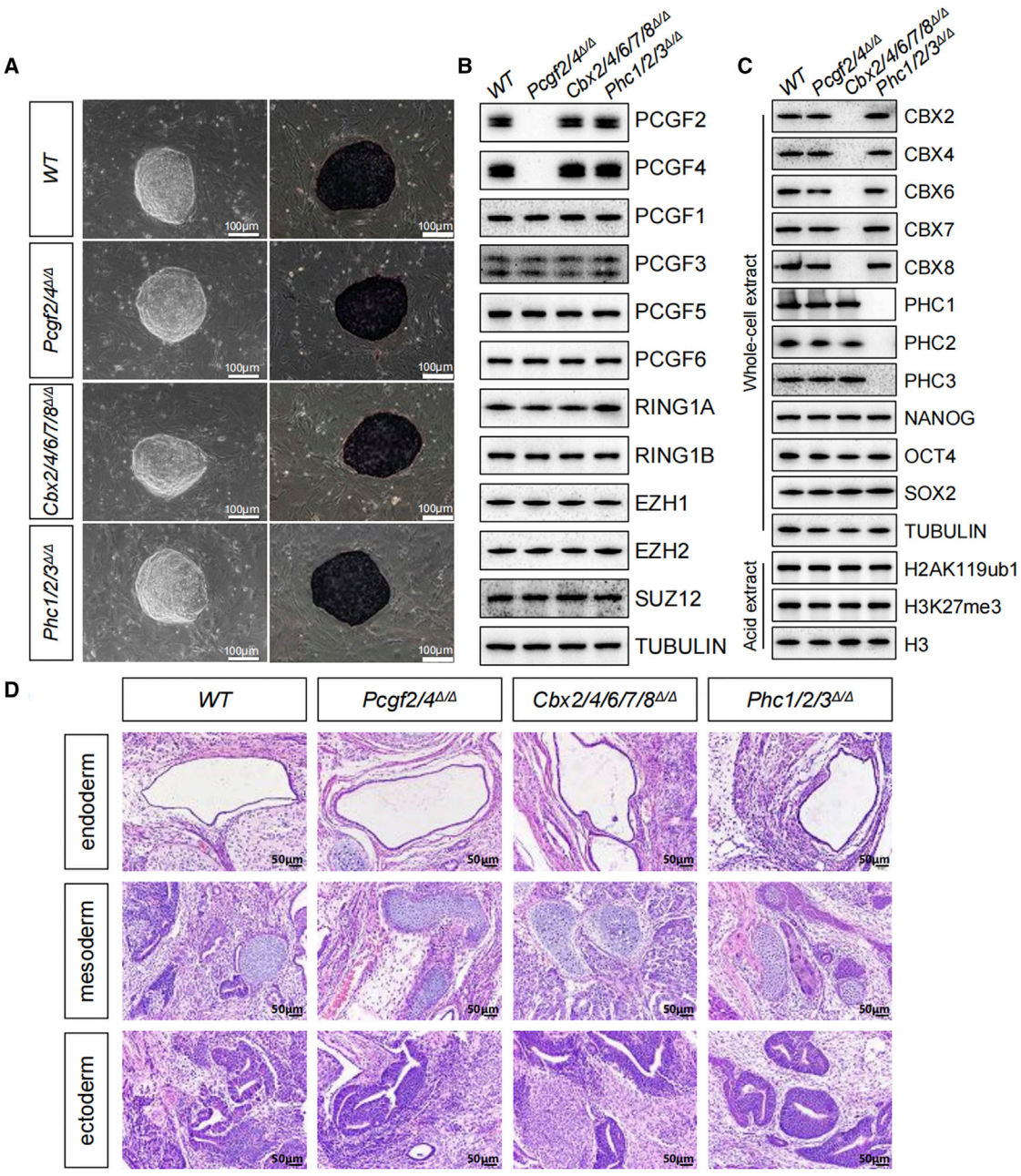

Figure 4. Individual disruption of cPRC1 does not induce exit from pluripotency in ESCs

(A) Phase-contrast images of ESC colonies on MEF feeders (left). Representative images of AP staining of WT and mutant ESC colonies of indicated genotypes (right).

(B and C) Western blot demonstrating changes in the levels of indicated PcG proteins, pluripotency factors, and histone modifications in ESCs of indicated genotypes. Tubulin and H3 were used as loading controls.

(D) Representative images showing H&E staining of histological sections derived from teratomas generated from ESCs of the indicated genotypes. Shown is a representative of three injected mice. Scale bars, 50 μm.

the ability to differentiate into all of the three main germ layers (Figures 4A–4D). Therefore, cPRC1 complexes are not the key determinant of self-renewal, and pluripotency in ESCs.

PCGF1/3/5/6 synergize to preserve ESC identity

Ablation of *Pcgf2/4* did not affect PcG-mediated pluripotency in ESCs, suggesting that the remaining PRC1 activities must be responsible for preserving the pluripotency (Figures

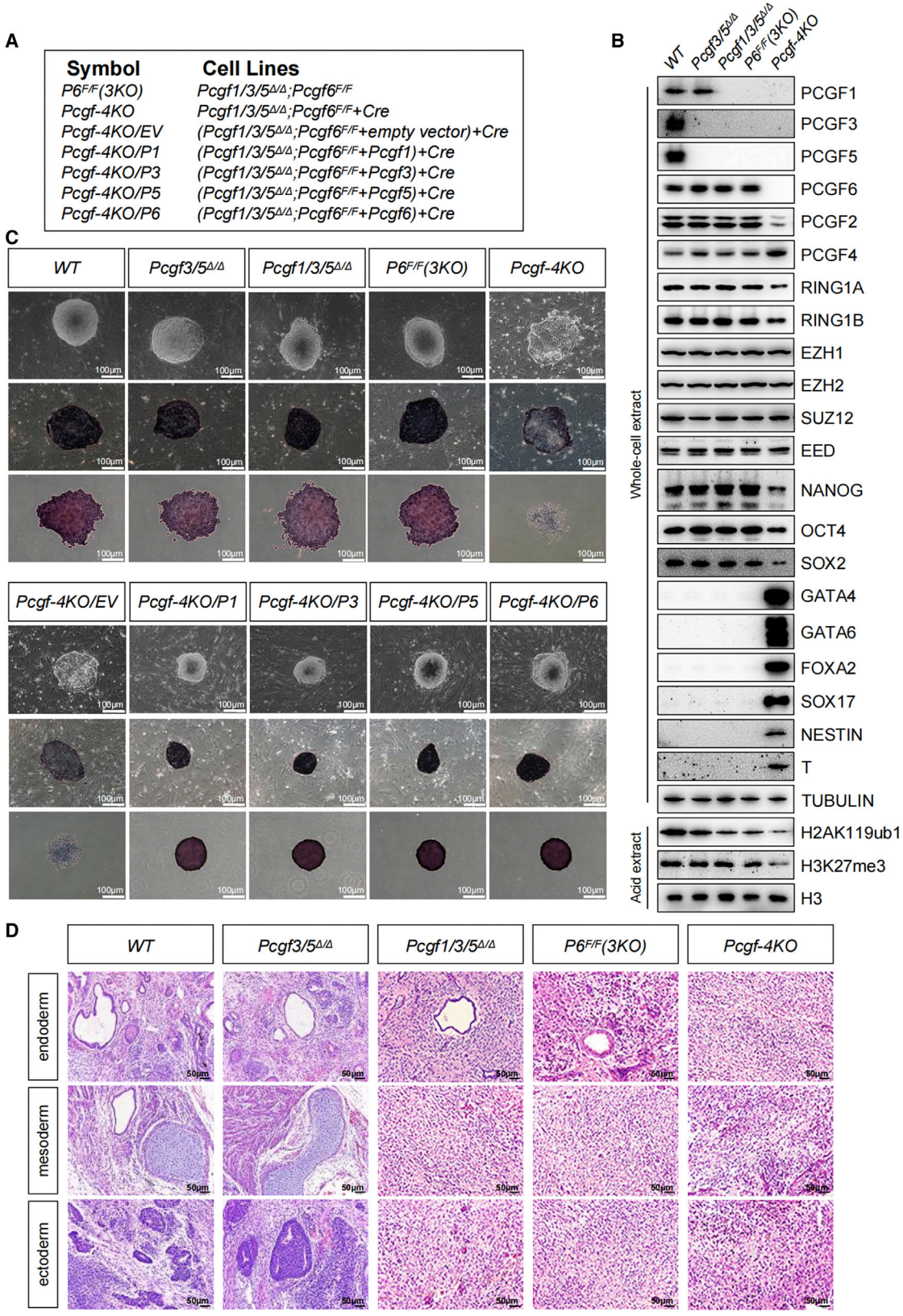

(legend on next page)

1B and 1C). Initially, we generated ESCs harboring double deletion of both *Pcgf3* and *Pcgf5* (*Pcgf3/5*$^{\Delta/\Delta}$), which participate in nearly identical protein complexes and would likely possess potential redundant functions. Consistent with previous observations (Zhao et al., 2017a), *Pcgf3/5*$^{\Delta/\Delta}$ did not lose ESC properties, nor do these cells show altered levels of pluripotency genes (Figures 5A–5C). Notably, although the global levels of H2AK119ub1 were not affected following removal of either *Pcgf3* or *Pcgf5*, loss of *Pcgf3/5* in combination caused a moderate reduction in H2AK119ub1, as evidenced by western blot (Figure 5B). As both PCGF1- and PCGF3/5-PRC1 complexes contributed to H2AK119ub1 (Fursova et al., 2019), we reasoned that PCGF1/3/5-PRC1 complexes may collaborate to support the pluripotency of ESCs. We therefore generated a triple knockout (*Pcgf1/3/5*$^{\Delta/\Delta}$) ESCs by simultaneous knockout of *Pcgf1/3/5*. Although removal of *Pcgf1/3/5* resulted in a further loss of H2AK119ub1 (Figure 5B), *Pcgf1/3/5*$^{\Delta/\Delta}$ ESCs formed round and compact colonies with typical undifferentiated ESC morphology indistinguishable from *Pcgf3/5*$^{\Delta/\Delta}$ colonies (Figure 5C). These colonies exhibited a high level of AP activity, as well as continuing to express ESC pluripotent markers (Figures 5B and 5C).

To circumvent the lethality or non-physiological responses associated with the deficiency for ncPRC1, we engineered *Pcgf1/3/5*$^{\Delta/\Delta}$ ESCs with conditional *Pcgf6*$^{F/F}$ (*Pcgf1/3/5*$^{\Delta/\Delta}$;*Pcgf6*$^{F/F}$) to eliminate all ncPRC1 activity. The established *Pcgf1/3/5*$^{\Delta/\Delta}$;*Pcgf6*$^{F/F}$ lines formed tightly compact colonies, stained mostly positive for AP, and continued to express high levels of pluripotency genes (Figures 5B and 5C). The introduction of Cre recombinase into the established *Pcgf1/3/5*$^{\Delta/\Delta}$;*Pcgf6*$^{F/F}$ lines led to the efficient ablation of PCGF6 proteins, yielding quadruple knockout (*Pcgf1/3/5/6*$^{\Delta/\Delta}$) cells that failed to maintain their pluripotent state, as determined by the reduced expression of key pluripotency factors at both the mRNA and protein levels (Figures 5B and 5C; Table S4). In concert with the reduced pluripotency factor expression, the *Pcgf1/3/5/6*$^{\Delta/\Delta}$ ESCs exhibited differentiated morphology and failed to be stained by AP (Figure 5C). Lineage-specific transcriptional regulators were aberrantly upregulated in those cells, consistent with the observed exit from the pluripotency state (Figure 5B). These results thus uncovered a previously unappreciated functional redundancy and cooperation among ncPRC1 complexes in preserving ESC pluripotent identity. Notably and consistent with a previous report (Fursova et al., 2019), ablation of *Pcgf6* in addition to *Pcgf1/3/5* caused a further reduction of H2AK119ub1 levels and a dramatic reduction in the levels of H3K27me3 (Figure 5B). In addition, while *Pcgf1/3/5/6*$^{\Delta/\Delta}$ ESCs displayed the same apoptotic rates as the control, cell-cycle analysis revealed these cells had a markedly extended G1 phase and a shortened S phase, suggesting that the impaired growth of *Pcgf1/3/5/6*$^{\Delta/\Delta}$ ESCs was due to the alteration of the cell cycle (Figures S5A and S5B). The functional redundancy among members of the ncPRC1-associated PCGF family was independently confirmed by exogenous expression of the ncPRC1-associated PCGF, which largely rescued the detrimental phenotype of *Pcgf1/3/5/6*$^{\Delta/\Delta}$ ESCs (Figures 5C, S5C, and S5D).

Pcgf3/5$^{\Delta/\Delta}$ maintained the ability to differentiate to derivatives of all three embryonic germ layers, whereas teratomas derived from *Pcgf1/3/5*$^{\Delta/\Delta}$ and *Pcgf1/3/5*$^{\Delta/\Delta}$;*Pcgf6*$^{F/F}$ ESCs did not contain more advanced ectodermal and mesodermal structures (Figures 5D, S5E, and S5F). Yet rare examples of differentiation into tissues from endodermal lineages could be found. Growth of *Pcgf1/3/5/6*$^{\Delta/\Delta}$ teratomas was delayed for several weeks (Figure S5E). In histologic analysis, the most abundant components of *Pcgf1/3/5/6*$^{\Delta/\Delta}$ teratomas were undifferentiated areas and featured a striking paucity of mature elements (Figures 5D and S5F). Consistent with these observations, *Pcgf1/3/5*$^{\Delta/\Delta}$ and *Pcgf1/3/5/6*$^{\Delta/\Delta}$ teratomas also showed strongly reduced expression of the three embryonic germ layer markers when compared with controls, as detected by qRT-PCR (Figure S5G). Therefore, our teratoma data strongly suggest that *Pcgf1/3/5/6*$^{\Delta/\Delta}$ ESCs are significantly impaired in their ability to differentiate properly. Remarkably, *Pcgf1/3/5/6-null* ESC lines can readily be propagated indefinitely in standard cell culture conditions. Together, ncPRC1 complexes, as opposed to cPRC1 complexes, play a fundamental and redundant role in maintaining pluripotency in ESCs.

cPRC1 and ncPRC1 collaborate to maintain the pluripotent state of ESCs

It is clear that *Pcgf1/3/5/6* loss failed to fully recapitulate the phenotype observed upon removal of *Ring1a/b*. We

Figure 5. Combined loss of *Pcgf1/3/5/6* unleash precocious differentiation of ESCs

(A) Reference legend for cell lines used in this figure and in Figure S5.

(B) Western blot demonstrating changes in the levels of selected PcG proteins, pluripotency factors, germ layer markers, H2AK119ub1, and H3K27me3 in ESCs of indicated genotypes. Tubulin and H3 were used as loading controls.

(C) Top: phase-contrast images of ESC colonies cultured on a layer of MEFs. Middle and bottom: representative images of AP staining of ESC colonies of indicated genotypes cultured together with a feeder layer of MEFs (middle) or on gelatin (bottom). Scale bar, 100 μm.

(D) H&E staining of teratoma sections revealed cells from various cell lineages including gut epithelium (endoderm), cartilage (mesoderm) and neural rosette (ectoderm). Shown is a representative of three injected mice. Scale bars, 50 μm.

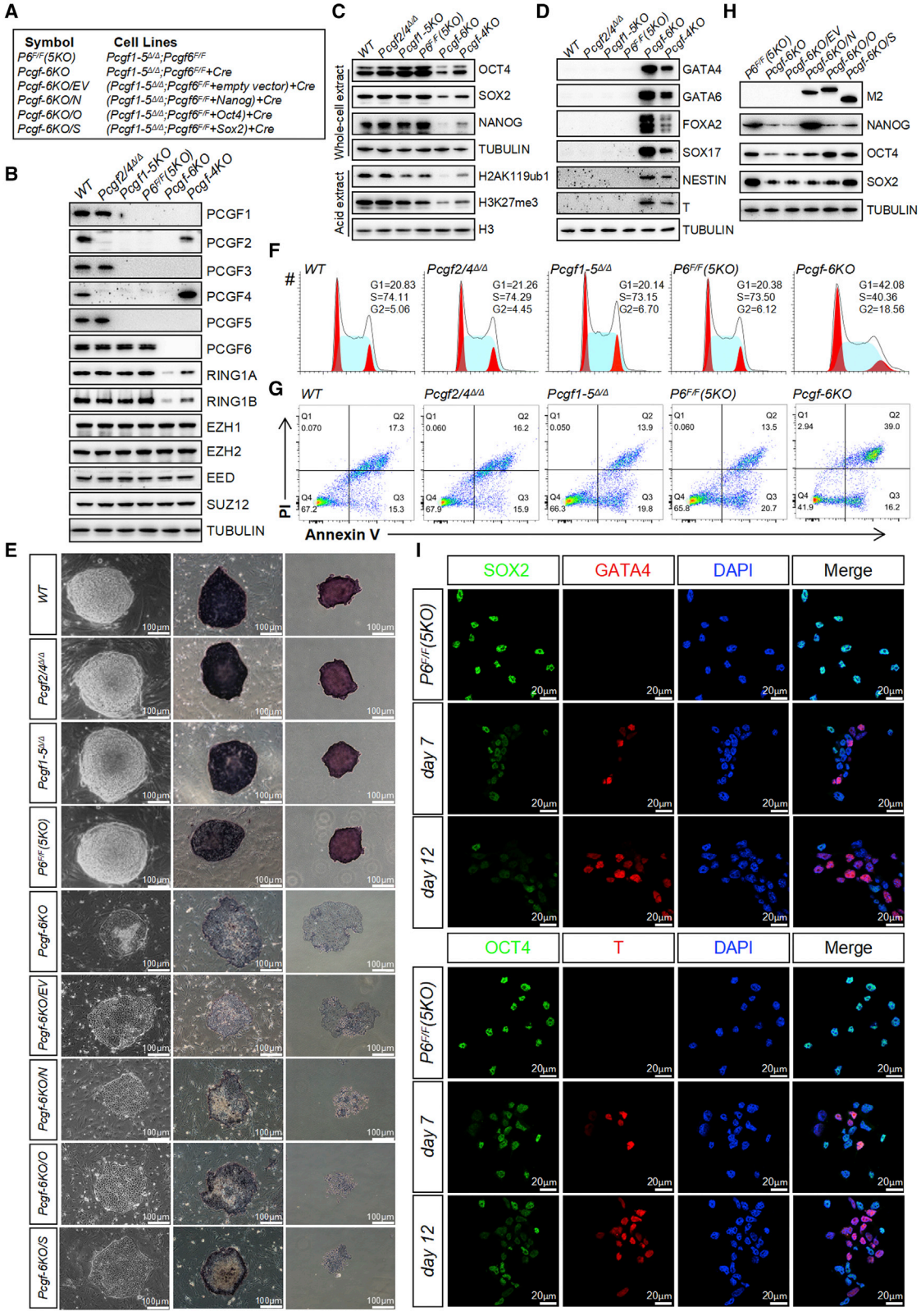

(legend on next page)

reasoned that ncPRC1 synergizes with cPRC1 to ensure robust maintenance of ESC pluripotency. To this end, we established *Pcgf1/3/5/2/4*$^{\Delta/\Delta}$ ESCs with conditional *Pcgf6*$^{F/F}$ (*Pcgf1/3/5/2/4*$^{\Delta/\Delta}$;*Pcgf6*$^{F/F}$) to eliminate all PRC1 activity (Figures 6A–6E). Interestingly, following removal of *Pcgf2/4* in addition to *Pcgf1/3/5*, no further reduction in global H2AK119ub1 levels was observed. In addition, *Pcgf1/3/5/2/4*$^{\Delta/\Delta}$ or *Pcgf1/3/5/2/4*$^{\Delta/\Delta}$;*Pcgf6*$^{F/F}$ ESCs formed colonies similar to those of undifferentiated *Pcgf1/3/5*$^{\Delta/\Delta}$ ESCs (Figure 6E). These cells also possessed AP activity and expressed high levels of OCT4, SOX2, and NANOG, supporting their pluripotent status (Figures 6C and 6E). Transfection of *Pcgf1/3/5/2/4*$^{\Delta/\Delta}$;*Pcgf6*$^{F/F}$ with a plasmid expressing the Cre recombinase resulted in the complete loss of PCGF6 protein and an almost complete loss of H2AK119ub1 (Figure 6C). Remarkably, Cre-mediated ablation of *Pcgf6* from *Pcgf1/3/5/2/4*$^{\Delta/\Delta}$;*Pcgf6*$^{F/F}$ ESCs resulted in a dramatic decrease in their rate of proliferation relative to control Cre-transfected cells. These effects were due to elevated apoptosis and G1/S cell-cycle arrest (Figures 6F and 6G). Upon plating of *Pcgf1-6*$^{\Delta/\Delta}$ cells onto a feeder layer, they underwent spontaneous differentiation, as evidenced by flattened and spreading morphology and by loss of AP staining (Figure 6E). The dramatic change in the colony morphology was accompanied by a drastic reduction in the expression of OCT4, SOX2, and NANOG (Figures 6C and 6I). Similar to *Ring1a/b*$^{\Delta/\Delta}$ cells, the phenotypes observed in *Pcgf1-6*$^{\Delta/\Delta}$ ESCs were not rescued by the ectopic expression of *Oct4*, *Sox2*, or *Nanog* (Figures 6E and 6H), and they could not be expanded beyond fourth passage and failed to form teratomas when implanted into immunodeficient mice (Figure 7A). The cellular phenotype in *Pcgf* sextuple knockout ESCs closely resembled those observed in *Ring1a/b*$^{\Delta/\Delta}$ ESCs, suggesting a vital role of PCGF family in regulating the stemness of ESCs.

Consistent with the observed phenotypes, we observed 4,994 (3,235 up, and 1,759 down) versus 7,491 (4,817 up, and 2,674 down) differentially expressed genes in *Pcgf1/3/5/6*$^{\Delta/\Delta}$ and *Pcgf1-6*$^{\Delta/\Delta}$ ESCs, respectively, compared with their corresponding controls (Figures 7B and 7C; Tables S4–S5). There was substantial overlap in genes deregulated in *Pcgf1/3/5/6*$^{\Delta/\Delta}$ and *Pcgf1-6*$^{\Delta/\Delta}$ ESCs; however, a large number of the genes deregulated in *Pcgf1-6*$^{\Delta/\Delta}$ but not *Pcgf1/3/5/6*$^{\Delta/\Delta}$ was observed (Figures 7D and 7E). GO analysis showed that among genes upregulated in *Pcgf1/3/5/6*$^{\Delta/\Delta}$ and *Pcgf1-6*$^{\Delta/\Delta}$ ESCs were genes related to pattern specification process, cell fate commitment, and tissue morphogenesis (Figure 7F). Processes related to developmental growth, chemotaxis, and cell-cell adhesion were over-represented among the genes downregulated in *Pcgf1/3/5/6*$^{\Delta/\Delta}$ and *Pcgf1-6*$^{\Delta/\Delta}$ cells. There was also significant overlap in genes deregulated between *Pcgf1/3/5/6*$^{\Delta/\Delta}$, *Pcgf1-6*$^{\Delta/\Delta}$ and *Ring1a/b*$^{\Delta/\Delta}$ cells; however, a large number of the genes deregulated in *Pcgf1-6*$^{\Delta/\Delta}$ but not *Ring1a/b*$^{\Delta/\Delta}$ was observed (Figures 7D and 7E). This suggests that both RING1A/B-dependent and -independent PCGF activities provide critical layers of gene regulation. Integration between RNA-seq and ChIP-seq data indicated that >38% and >30% of the deregulated genes in *Pcgf1/3/5/6*$^{\Delta/\Delta}$ and *Pcgf1-6*$^{\Delta/\Delta}$, respectively, were direct targets of PRC1. Intriguingly, GO analysis revealed that these direct PRC1 targets were enriched for pattern specification process, cell fate commitment, embryonic morphogenesis, and negative regulation of cell differentiation (Figure S6). By performing qRT-PCR, western blot analysis and IF, we confirmed the RNA-seq finding and observed that ablation of both Polycomb complexes had an additive effect on the expression levels of lineage-affiliated genes (Figures 6D, 6I, and 7G). Altogether, we conclude that cPRC1 and ncPRC1 act redundantly to suppress lineage-specific genes and preserve ESC identity.

As shown in Figure 6B, *Pcgf1/3/5/6* and *Pcgf1-6* deletion led to a moderate and substantial reduction, respectively, in the protein levels of RING1A and RING1B, whereas loss of *Pcgf2/4* did not appear to appreciably affect the protein levels of RING1A and RING1B. However, RNA-seq analysis demonstrated that ablation of *Pcgf1/3/5/6* or *Pcgf1-6* did not alter steady-state levels of *Ring1a* and

Figure 6. Simultaneous ablation of cPRC1 and ncPRC1 triggers spontaneous differentiation and loss of self-renewal

(A) Reference legend for cell lines used in this figure and in Figure 7.

(B–D) Western blot demonstrating changes in the levels of selected (B) PcG proteins, (C) pluripotency factors, histone modifications, and (D) germ layer markers in ESCs of indicated genotypes. Tubulin and H3 were used as loading controls.

(E) Left: phase-contrast images of ESC colonies of indicated genotypes cultured on a feeder layer. Middle and right: images of ESC colonies cultured on feeder layers (middle) or gelatin (right) after AP staining. Scale bar, 100 μm.

(F) Representative cell-cycle profiles determined by propidium iodide (PI) staining and FACS analysis.

(G) Flow cytometric quantification of apoptosis with Annexin V and PI. The percentages of Annexin V-positive (apoptotic) cells are within the two right quadrants.

(H) Western blot analyses using the indicated antibodies on whole-cell lysates from ESCs of indicated genotypes. The expression levels of the indicated FLAG-tagged proteins were detected with anti-Flag M2 antibody.

(I) IF analysis for SOX2, OCT4 (green), GATA4, T (red), or DAPI (blue) in *Pcgf1-5*$^{\Delta/\Delta}$;*Pcgf6*$^{F/F}$ ESCs following lenti-Cre infection. Images were taken at 63× magnification using confocal microscopy. Merge, merged images.

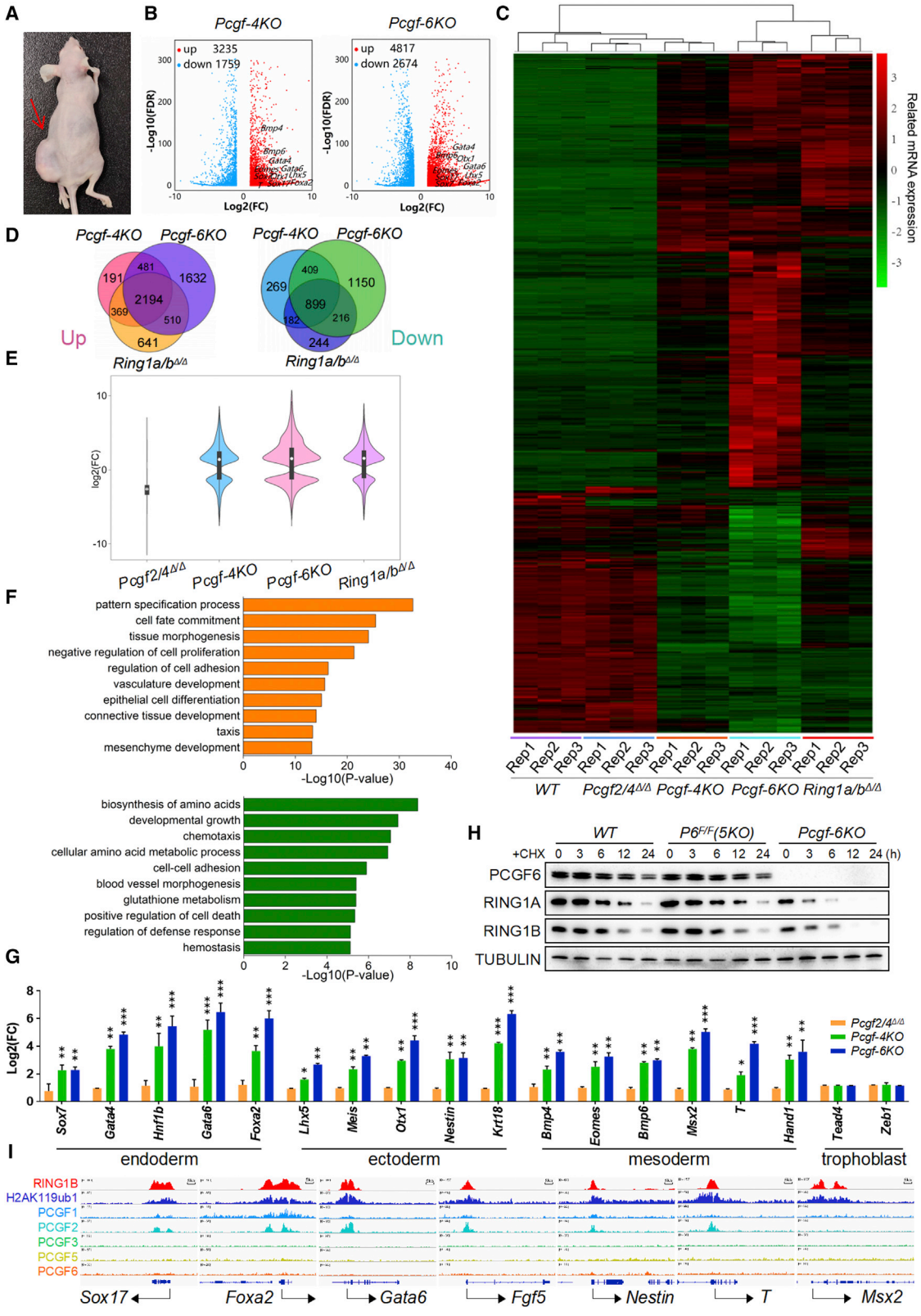

(legend on next page)

Ring1b mRNA in ESCs (Tables S4–S5), suggesting a mechanism involving posttranscriptional regulation. A time-course cycloheximide (CHX) experiment revealed that RING1A and RING1B protein half-lives were markedly decreased, from approximately 4 and 6 h in *Pcgf1/3/5/2/4*$^{\Delta/\Delta}$;*Pcgf6*$^{F/F}$ ESCs to less than 2 and 3 h, respectively, in *Pcgf1-6*$^{\Delta/\Delta}$ cells (Figure 7H), suggesting that PCGF family members act redundantly to increases RING1A and RING1B protein stability. In line with these results, a cohort of key lineage-specific genes, which were upregulated in *Pcgf1-6*$^{\Delta/\Delta}$ ESCs and possessed a high enrichment of RING1B, PCGF2, and H2AK119ub1, were not or only weakly targeted by the ncPRC1-associated PCGF proteins (Figure 7I). Collectively, these findings provide novel evidence to suggest how the action of PCGF family on RING1A/B stability and resultant activity could impact on ESC fate decisions.

DISCUSSION

Self-renewing ESCs are derived from the ICM of the pre-implantation blastocyst (Evans and Kaufman, 1981; Martin, 1981). They are regarded as an excellent model system for analyzing the mechanisms governing cell fate transitions during early embryo development. The hallmark characteristics of ESCs is their pluripotency, which bestows them with a capacity to give rise to all cell types of the body. The lineage-specific differentiation of ESCs *in vitro* closely recapitulates the lineage commitment in the embryo that occurs *in vivo*. The mechanisms responsible for the maintenance of ESC pluripotency, and those that guide their commitment into particular cell lineages, remain to be further explored. In ESCs, PcG proteins bind preferentially to genes encoding lineage-specific transcription factors to prevent both exit from pluripotency and premature differentiation (Boyer et al., 2006). Uncovering the underlying mechanism of PcG-mediated pluripotency maintenance remains challenging due to the multiple possible combinatorial permutations within PRC1 complexes (Gao et al., 2012; Hauri et al., 2016).

The catalytic core of PRC1 is formed by RING1A/B and one of six PCGF partners, giving rise to an array of biochemically distinct cPRC1 or ncPRC1 complexes (Gao et al., 2012). Inactivation of *Ring1a* results in fertile mice with minor skeletal alterations (del Mar Lorente et al., 2000). In contrast, disruption of *Ring1b* in mice causes embryonic lethality due to gastrulation arrest (Voncken et al., 2003). Whereas RING1A and RING1B can have redundant functions during development (del Mar Lorente et al., 2000; Voncken et al., 2003), the combined deletion of *Ring1a/b* causes developmental arrest before the two-cell stage (Posfai et al., 2012), highlighting the requirement to genetically delete both genes to fully characterize PRC1 biological roles. Intriguingly, this also corresponds with the relative importance for maintenance of H2AK119ub1 and pluripotency of these Ring E3 ligases as RING1A or RING1B loss has no or only mild effect on H2AK119ub1 levels and the property of ESCs, whereas simultaneous depletion of *Ring1a/b* results in a full loss of H2AK119ub1 and of pluripotency and commitment toward lineages of the three germ layers with loss of indefinite self-renewal (Figures 3 and S2).

cPRC1 complexes, which are recruited to specific genomic sites via recognition of H3K27me3 deposited by PRC2, have been proposed to be involved in the Polycomb-mediated gene silencing (Schuettengruber et al., 2017). However, recent studies have documented that loss of cPRC1 complexes has little or no effect on gene expression (Fursova et al., 2019; Zepeda-Martinez et al., 2020). Consistently, we found that removal of *Pcgf2/4* in ESCs has no discernible effect on the maintenance of

Figure 7. cPRC1 and ncPRC1 act redundantly to silence lineage-specific genes

(A) Representative images of mice bearing teratomas 28 days after the injection of *Pcgf1/3/5/2/4*$^{\Delta/\Delta}$;*Pcgf6*$^{F/F}$ (left side, indicated by a red arrow) or *Pcgf1-6*$^{\Delta/\Delta}$ ESCs (right side). Four mice were injected per condition.

(B) Volcano plots of −log10 (p value) against log2-fold change representing the differences in gene expression in ESCs of indicated genotypes. Upregulated (red) and downregulated (blue) genes are highlighted.

(C) Heatmap illustrating fold changes in gene expression in ESCs of indicated genotypes. False discovery rate <0.05. Up- and downregulated genes are reported as red and green, respectively.

(D) Venn diagram showing overlap of upregulated (left) or downregulated (right) genes between *Pcgf-4KO*, *Pcgf-6KO*, and *Ring1a/b*$^{\Delta/\Delta}$ ESCs. (E) A violin plot comparing log2-fold changes of genes in ESCs deficient for *Pcgf2/4*, *Pcgf1/3/5/6*, *Pcgf1-6*, and *Ring1a/b*.

(F) Gene ontology analysis of overlapping genes upregulated (top) and downregulated (bottom) between *Pcgf-4KO* and *Pcgf-6KO* ESCs.

(G) qRT-PCR of germ layer markers, measured in *WT*, *Pcgf-4KO*, and *Pcgf-6KO* ESCs. Each value was normalized to actin expression, and for each gene the expression level in the wild-type ESCs was arbitrarily set to 1.

(H) ESCs of indicated genotypes were treated with cycloheximide (CHX) as indicated and lysates were blotted with the indicated antibodies. Tubulin was used as a loading control.

(I) Genomic snapshots of the indicated ChIP-seq profiles at selected germ layer gene loci in WT ESCs. Published ChIP-seq data were obtained from NCBI GEO (accession numbers GSE122715 and GSE107377). Data in (G) represent the mean ± SD of three independent experiments. *p < 0.05, **p < 0.01, ***p < 0.001 (Student's t test) compared with the control.

pluripotency (Figure 4). In line with these observations, mice harboring inactivating mutations of cPRC1 components exhibit only minor or delayed defects in embryogenesis (Akasaka et al., 2001; Coré et al., 1997; Forzati et al., 2012; Isono et al., 2005; Lau et al., 2017). In contrast, targeted disruptions to ncPRC1 in mice result in early embryonic lethality (Almeida et al., 2017; Endoh et al., 2017; Liu et al., 2020; Pirity et al., 2005; Qin et al., 2012; Washkowitz et al., 2015). *In vitro* differentiation assays indicated that knockout of single *Pcgf* in ESCs resulted in moderate defects affecting the proper formation of the three germ layers (Endoh et al., 2017; Morey et al., 2015; Yan et al., 2017; Zhao et al., 2017a, 2017b). However, these single mutant cells have the potential to form teratomas composed of derivatives from all three germ layers *in vivo* (Figure 2), suggesting that inactivation of individual *Pcgf* family members has no significant effect on the maintenance of ESC identity. Loss of ncPRC1 core subunits PCGF1/3/5/6 triggered the spontaneous differentiation and derepression of lineage-specific genes, suggesting a redundant but essential role of PCGF family in maintaining ESC pluripotency (Figure 5). These phenotypic discrepancies between cPRC1 and ncPRC1 could reflect distinct roles in ESC identity maintenance. Alternatively, cPRC1-dependent and cPRC1-independent PRC1 complexes might play redundant roles in ESC fate specification. Interestingly, lineage-specific genes were strongly derepressed in the *Pcgf1-6* knockout cells compared with *Pcgf2/4* or *Pcgf1/3/5/6* knockouts, where they largely remained repressed or were moderately derepressed, respectively. In addition, loss of ESC self-renewal capacity is achieved only when both cPRC1- and ncPRC1-associated PCGF proteins are ablated (Figure 6). Together, our findings demonstrate that cPRC1 and ncPRC1 function redundantly to silence unwanted lineage-specific genes and safeguard against exit from ESC pluripotency.

Our functional interrogation of PRC1 activity indicates that redundancy among distinct PRC1 complexes is central to PcG-mediated cell fate specification in ESCs. This is somewhat surprising given that exogenously expressed HA-tagged PCGF proteins in 293T cells occupy mutually exclusive regions of the genome, possibly arguing against redundancy among different PRC1 complexes (Gao et al., 2012). In contrast, genomic profiling of endogenous PCGF proteins in ESCs reveals that ncPRC1 complexes, as opposed to cPRC1 complexes, largely co-occupy target regions, where they act synergistically to shape genomic H2AK119ub1 and define gene repression (Fursova et al., 2019). Interestingly, another group reported that PCGF1/2/4 jointly preserve H2AK119ub1 deposition at common targets even though PCGF proteins display high binding specificity (Scelfo et al., 2019). By using combinatorial genetic perturbation coupled with functional evaluation, our findings reconcile these apparent discrepancies leading to the interpretation that ncPRC1 complexes, but not cPRC1 complexes, predominantly define PcG-mediated cell fate specification in ESCs (Figure 5). Most importantly, we discover that genetic ablation of both cPRC1 and ncPRC1 largely phenocopies lineage-specific gene repression and cellular defects caused by complete loss of PRC1 in ESCs via ablation of *Ring1a/b* (Figures 3 and 6). This suggests that, although biochemically distinct PRC1 subcomplexes display high binding specificity, which enables them to function at defined sites in the genome, for example, PRC1.6 at germ cell-related genes (Endoh et al., 2017; Qin et al., 2012, 2021; Stielow et al., 2018), they also co-occupy target sites, where they act redundantly to deposit genomic H2AK119ub1 and define lineage-specific gene repression. Critically, we provide novel evidence to suggest how the action of PCGF family members on RING1A/B stability could impact on ESC fate determination. These findings underscore the need to further explore the mechanisms that control the levels and activity of RING1A/B in ESCs. Overall, our discoveries provide compelling evidence of functional redundancy between cPRC1 and ncPRC1 in robust repression of key lineage-specific genes, which is required for governing ESC identity.

EXPERIMENTAL PROCEDURES

Plasmid construction and generation of mutant cell lines

sgRNAs were designed based on the CRISPR design website (http://crispor.tefor.net/). A pair of 20-bp oligonucleotides was annealed and inserted into the *Bbs*I-digested Cas9 and sgRNA-expressing PX459 vector (Addgene plasmid no. 62988; http://n2t.net/addgene: 62988; RRID: Addgene_62988), which was resistant to puromycin. sgRNA-expressing plasmids were verified by DNA sequencing. Constructed plasmids were transfected into ESCs by Lipofectamine 2000 (Life Technologies) according to the manufacturer's instructions. Twenty-four hours after transfection, puromycin-resistant ESCs were selected for 48 h and then grown on mitomycin-treated feeder. Subsequently, ESC colonies were picked and screened by gnomic PCR, and confirmed by RT-PCR and western blot. Conditional knockout ESC mutants were performed as described previously (Qin et al., 2021). Details of the mutant ESC lines used in this study are listed in Table S6. All of the primers and antibodies used in this study are listed in Table S7 or in a previous report (Qin et al., 2021).

Statistics

Unless stated otherwise, all data were shown as mean values ± SD or mean values ± SEM for experiments performed with at least three independent experiments. GraphPad Prism 5 was used to perform statistical tests and generate p values using two-tailed Student's t test for comparisons between two datasets, and p values of less than 0.05 were considered statistically significant. Statistical significance was

presented in figures in the following manner: *p < 0.05, **p < 0.01, ***p < 0.001.

Data and code availability

The accession number for the sequencing data reported in this paper is NCBI GEO: GEO183646. All other data needed to evaluate the conclusions in the paper are present in the paper and/or the supplementary material. All original data, including images and mutant lines, pertaining to this study will be made available upon request.

SUPPLEMENTAL INFORMATION

Supplemental information can be found online at https://doi.org/10.1016/j.stemcr.2022.02.020.

AUTHOR CONTRIBUTIONS

Conceptualization, J.Q.; methodology, Y.Z., L.D., C.W., K.H., L.Z., and J.Q.; formal analysis, Y.Z., L.D., C.W., K.H., J.W., L.X., and J.Q.; mechanistic investigations, Y.Z., L.D., C.W., Y.X., Q.J., and J.Q.; writing – original draft, J.Q.; writing – review & editing, J.Q., Y.Z., L.D., and C.W.; funding acquisition, J.Q.; supervision, J.Q.

CONFLICT OF INTEREST

The authors declare no competing interests.

ACKNOWLEDGMENTS

We are indebted to all members of the Qin laboratory and to Yikai Huang and Ting Su for experimental advice and helpful discussions. This work was supported by grants from the National Natural Science Foundation of China (31970810) to J.Q.

Received: September 22, 2021
Revised: February 27, 2022
Accepted: February 28, 2022
Published: March 31, 2022

REFERENCES

Akasaka, T., van Lohuizen, M., van der Lugt, N., Mizutani-Koseki, Y., Kanno, M., Taniguchi, M., Vidal, M., Alkema, M., Berns, A., and Koseki, H. (2001). Mice doubly deficient for the Polycomb Group genes Mel18 and Bmi1 reveal synergy and requirement for maintenance but not initiation of Hox gene expression. Development *128*, 1587–1597.

Almeida, M., Pintacuda, G., Masui, O., Koseki, Y., Gdula, M., Cerase, A., Brown, D., Mould, A., Innocent, C., Nakayama, M., et al. (2017). PCGF3/5-PRC1 initiates Polycomb recruitment in X chromosome inactivation. Science *356*, 1081–1084.

Boyer, L.A., Lee, T.I., Cole, M.F., Johnstone, S.E., Levine, S.S., Zucker, J.P., Guenther, M.G., Kumar, R.M., Murray, H.L., Jenner, R.G., et al. (2005). Core transcriptional regulatory circuitry in human embryonic stem cells. Cell *122*, 947–956.

Boyer, L.A., Plath, K., Zeitlinger, J., Brambrink, T., Medeiros, L.A., Lee, T.I., Levine, S.S., Wernig, M., Tajonar, A., Ray, M.K., et al. (2006). Polycomb complexes repress developmental regulators in murine embryonic stem cells. Nature *441*, 349–353.

Coré, N., Bel, S., Gaunt, S.J., Aurrand-Lions, M., Pearce, J., Fisher, A., and Djabali, M. (1997). Altered cellular proliferation and mesoderm patterning in Polycomb-M33-deficient mice. Development *124*, 721–729.

del Mar Lorente, M., Marcos-Gutiérrez, C., Pérez, C., Schoorlemmer, J., Ramírez, A., Magin, T., and Vidal, M. (2000). Loss- and gain-of-function mutations show a polycomb group function for Ring1A in mice. Development *127*, 5093–5100.

Dickinson, M.E., Flenniken, A.M., Ji, X., Teboul, L., Wong, M.D., White, J.K., Meehan, T.F., Weninger, W.J., Westerberg, H., Adissu, H., et al. (2016). High-throughput discovery of novel developmental phenotypes. Nature *537*, 508–514.

Endoh, M., Endo, T.A., Shinga, J., Hayashi, K., Farcas, A., Ma, K.W., Ito, S., Sharif, J., Endoh, T., Onaga, N., et al. (2017). PCGF6-PRC1 suppresses premature differentiation of mouse embryonic stem cells by regulating germ cell-related genes. Elife *6*, e21064.

Evans, M.J., and Kaufman, M.H. (1981). Establishment in culture of pluripotential cells from mouse embryos. Nature *292*, 154–156.

Forzati, F., Federico, A., Pallante, P., Abbate, A., Esposito, F., Malapelle, U., Sepe, R., Palma, G., Troncone, G., Scarfò, M., et al. (2012). CBX7 is a tumor suppressor in mice and humans. J. Clin. Invest. *122*, 612–623.

Fursova, N.A., Blackledge, N.P., Nakayama, M., Ito, S., Koseki, Y., Farcas, A.M., King, H.W., Koseki, H., and Klose, R.J. (2019). Synergy between variant PRC1 complexes defines polycomb-mediated gene repression. Mol. Cell *74*, 1020–1036.e1028.

Gao, Z., Zhang, J., Bonasio, R., Strino, F., Sawai, A., Parisi, F., Kluger, Y., and Reinberg, D. (2012). PCGF homologs, CBX proteins, and RYBP define functionally distinct PRC1 family complexes. Mol. Cell *45*, 344–356.

Hauri, S., Comoglio, F., Seimiya, M., Gerstung, M., Glatter, T., Hansen, K., Aebersold, R., Paro, R., Gstaiger, M., and Beisel, C. (2016). A high-density map for navigating the human polycomb complexome. Cell Rep. *17*, 583–595.

Isono, K., Fujimura, Y., Shinga, J., Yamaki, M., J, O.W., Takihara, Y., Murahashi, Y., Takada, Y., Mizutani-Koseki, Y., and Koseki, H. (2005). Mammalian polyhomeotic homologues Phc2 and Phc1 act in synergy to mediate polycomb repression of Hox genes. Mol. Cell. Biol. *25*, 6694–6706.

Lau, M.S., Schwartz, M.G., Kundu, S., Savol, A.J., Wang, P.I., Marr, S.K., Grau, D.J., Schorderet, P., Sadreyev, R.I., Tabin, C.J., et al. (2017). Mutation of a nucleosome compaction region disrupts Polycomb-mediated axial patterning. Science *355*, 1081–1084.

Liu, M., Zhu, Y., Xing, F., Liu, S., Xia, Y., Jiang, Q., and Qin, J. (2020). The polycomb group protein PCGF6 mediates germline gene silencing by recruiting histone-modifying proteins to target gene promoters. J. Biol. Chem. *295*, 9712–9724.

Martin, G.R. (1981). Isolation of a pluripotent cell line from early mouse embryos cultured in medium conditioned by teratocarcinoma stem cells. Proc. Natl. Acad. Sci. U S A *78*, 7634–7638.

Morey, L., Santanach, A., Blanco, E., Aloia, L., Nora, E.P., Bruneau, B.G., and Di Croce, L. (2015). Polycomb regulates mesoderm cell

fate-specification in embryonic stem cells through activation and repression mechanisms. Cell Stem Cell *17*, 300–315.

Pirity, M.K., Locker, J., and Schreiber-Agus, N. (2005). Rybp/DEDAF is required for early postimplantation and for central nervous system development. Mol. Cell. Biol. *25*, 7193–7202.

Piunti, A., and Shilatifard, A. (2021). The roles of Polycomb repressive complexes in mammalian development and cancer. Nat. Rev. Mol. Cel. Biol. *22*, 326–345.

Posfai, E., Kunzmann, R., Brochard, V., Salvaing, J., Cabuy, E., Roloff, T.C., Liu, Z., Tardat, M., van Lohuizen, M., Vidal, M., et al. (2012). Polycomb function during oogenesis is required for mouse embryonic development. Genes Dev. *26*, 920–932.

Qin, J., Wang, C., Zhu, Y., Su, T., Dong, L., Huang, Y., and Hao, K. (2021). Mga safeguards embryonic stem cells from acquiring extraembryonic endoderm fates. Sci. Adv. *7*, eabe5689.

Qin, J., Whyte, W.A., Anderssen, E., Apostolou, E., Chen, H.H., Akbarian, S., Bronson, R.T., Hochedlinger, K., Ramaswamy, S., Young, R.A., et al. (2012). The polycomb group protein L3mbtl2 assembles an atypical PRC1-family complex that is essential in pluripotent stem cells and early development. Cell Stem Cell *11*, 319–332.

Saurin, A.J., Shao, Z., Erdjument-Bromage, H., Tempst, P., and Kingston, R.E. (2001). A Drosophila Polycomb group complex includes Zeste and dTAFII proteins. Nature *412*, 655–660.

Scelfo, A., Fernández-Pérez, D., Tamburri, S., Zanotti, M., Lavarone, E., Soldi, M., Bonaldi, T., Ferrari, K.J., and Pasini, D. (2019). Functional landscape of PCGF proteins reveals both RING1A/B-Dependent-and RING1A/B-Independent-Specific activities. Mol. Cell *74*, 1037–1052.e1037.

Schuettengruber, B., Bourbon, H.M., Di Croce, L., and Cavalli, G. (2017). Genome regulation by polycomb and Trithorax: 70 Years and counting. Cell *171*, 34–57.

Shao, Z., Raible, F., Mollaaghababa, R., Guyon, J.R., Wu, C.T., Bender, W., and Kingston, R.E. (1999). Stabilization of chromatin structure by PRC1, a Polycomb complex. Cell *98*, 37–46.

Simon, J.A., and Kingston, R.E. (2009). Mechanisms of polycomb gene silencing: knowns and unknowns. Nat. Rev. Mol. Cel. Biol. *10*, 697–708.

Stielow, B., Finkernagel, F., Stiewe, T., Nist, A., and Suske, G. (2018). MGA, L3MBTL2 and E2F6 determine genomic binding of the noncanonical Polycomb repressive complex PRC1.6. PLoS Genet. *14*, e1007193.

Voncken, J.W., Roelen, B.A., Roefs, M., de Vries, S., Verhoeven, E., Marino, S., Deschamps, J., and van Lohuizen, M. (2003). Rnf2 (Ring1b) deficiency causes gastrulation arrest and cell cycle inhibition. Proc. Natl. Acad. Sci. U S A *100*, 2468–2473.

Washkowitz, A.J., Schall, C., Zhang, K., Wurst, W., Floss, T., Mager, J., and Papaioannou, V.E. (2015). Mga is essential for the survival of pluripotent cells during peri-implantation development. Development *142*, 31–40.

Yan, Y., Zhao, W., Huang, Y., Tong, H., Xia, Y., Jiang, Q., and Qin, J. (2017). Loss of polycomb group protein Pcgf1 severely compromises proper differentiation of embryonic stem cells. Scientific Rep. *7*, 46276.

Zepeda-Martinez, J.A., Pribitzer, C., Wang, J., Bsteh, D., Golumbeanu, S., Zhao, Q., Burkard, T.R., Reichholf, B., Rhie, S.K., Jude, J., et al. (2020). Parallel PRC2/cPRC1 and vPRC1 pathways silence lineage-specific genes and maintain self-renewal in mouse embryonic stem cells. Sci. Adv. *6*, eaax5692.

Zhao, W., Huang, Y., Zhang, J., Liu, M., Ji, H., Wang, C., Cao, N., Li, C., Xia, Y., Jiang, Q., et al. (2017a). Polycomb group RING finger proteins 3/5 activate transcription via an interaction with the pluripotency factor Tex10 in embryonic stem cells. J. Biol. Chem. *292*, 21527–21537.

Zhao, W., Tong, H., Huang, Y., Yan, Y., Teng, H., Xia, Y., Jiang, Q., and Qin, J. (2017b). Essential role for polycomb group protein Pcgf6 in embryonic stem cell maintenance and a noncanonical polycomb repressive complex 1 (PRC1) integrity. J. Biol. Chem. *292*, 2773–2784.

Stem Cell Reports, Volume *17*

Supplemental Information

Functional redundancy among Polycomb complexes in maintaining the pluripotent state of embryonic stem cells

Yaru Zhu, Lixia Dong, Congcong Wang, Kunying Hao, Jingnan Wang, Linchun Zhao, Lijun Xu, Yin Xia, Qing Jiang, and Jinzhong Qin

Supplementary Materials for

Functional redundancy among Polycomb complexes in maintaining the pluripotent state of embryonic stem cells

Yaru Zhu[1†], Lixia Dong[1†], Congcong Wang[1†], Kunying Hao[1†], Jingnan Wang[1], Linchun Zhao[1], Lijun Xu[1], Yin Xia[2], Qing Jiang[3], Jinzhong Qin[1,4*]

*Correspondence author. Email: qinjz@nju.edu.cn

The PDF file includes:

Figs. S1 to S6

Tables S6 to S8

Other Supplementary Material for this manuscript includes the following:

Tables S1 to S5

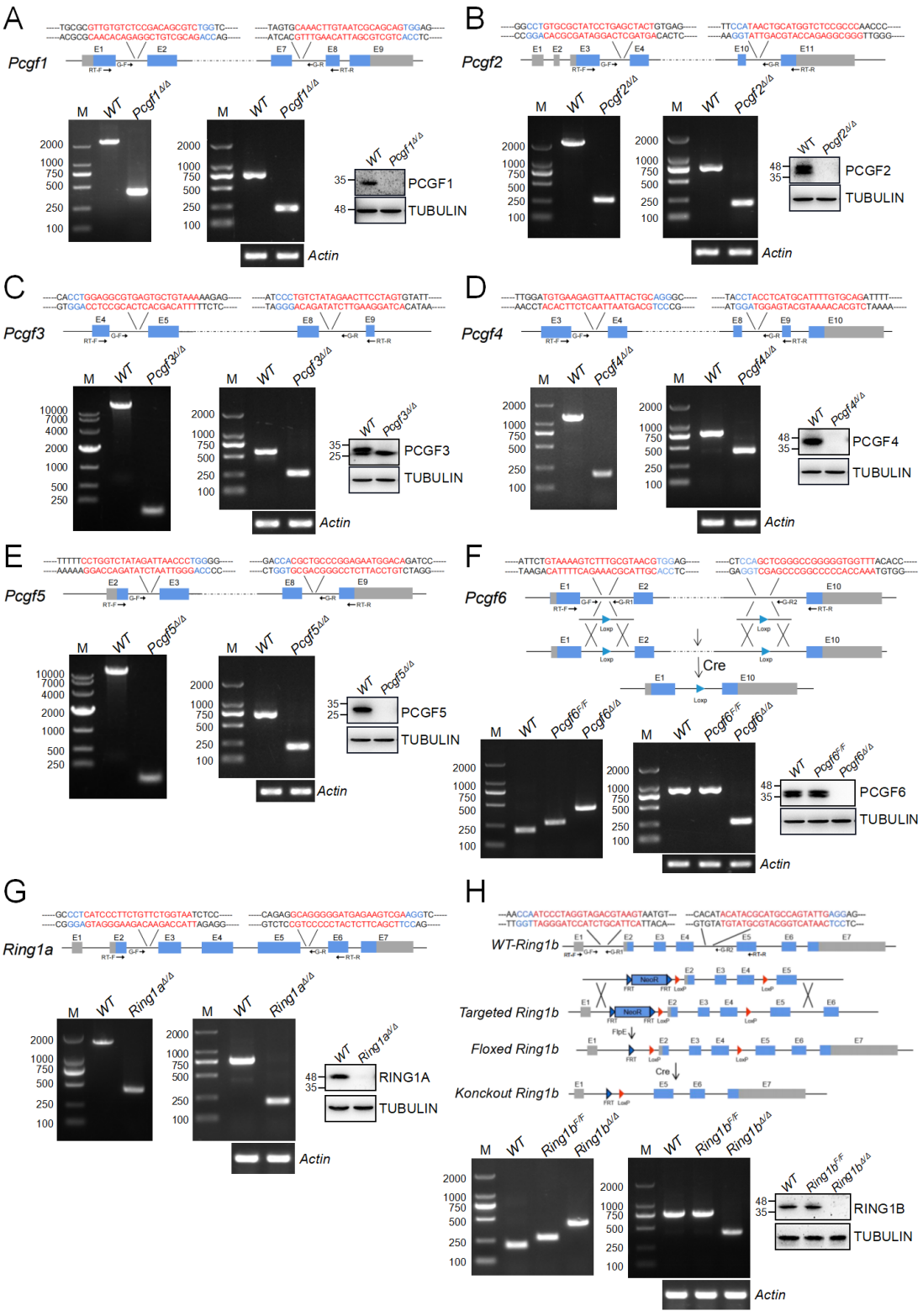

Figure S1. Generation of knockout ESC lines of *Pcgf* family, *Ring1a* and *Ring1b*. Related to Figures 1 to 3. (**A** to **H**) Top, schematic representation of CRISPR/Cas9 mediated knockout approaches to generate ESCs deficient in *Pcgf* family, *Ring1a* and *Ring1b*. PAM sequences are in blue following the sgRNA sequence highlighted in red. The locations of genomic PCR primers (G-F, Forward; G-R, Reverse) and RT-PCR primers (RT-F, Forward; RT-R, Reverse) are shown. Bottom, genotyping of ESCs with

indicated gene deletions using primers located upstream and downstream of the deleted region (left); RT-PCR analysis for residual mRNA revealed a shorter band in the mutants (middle). The absence of the protein is confirmed by using western blot (right).TUBULIN acted as a loading control.

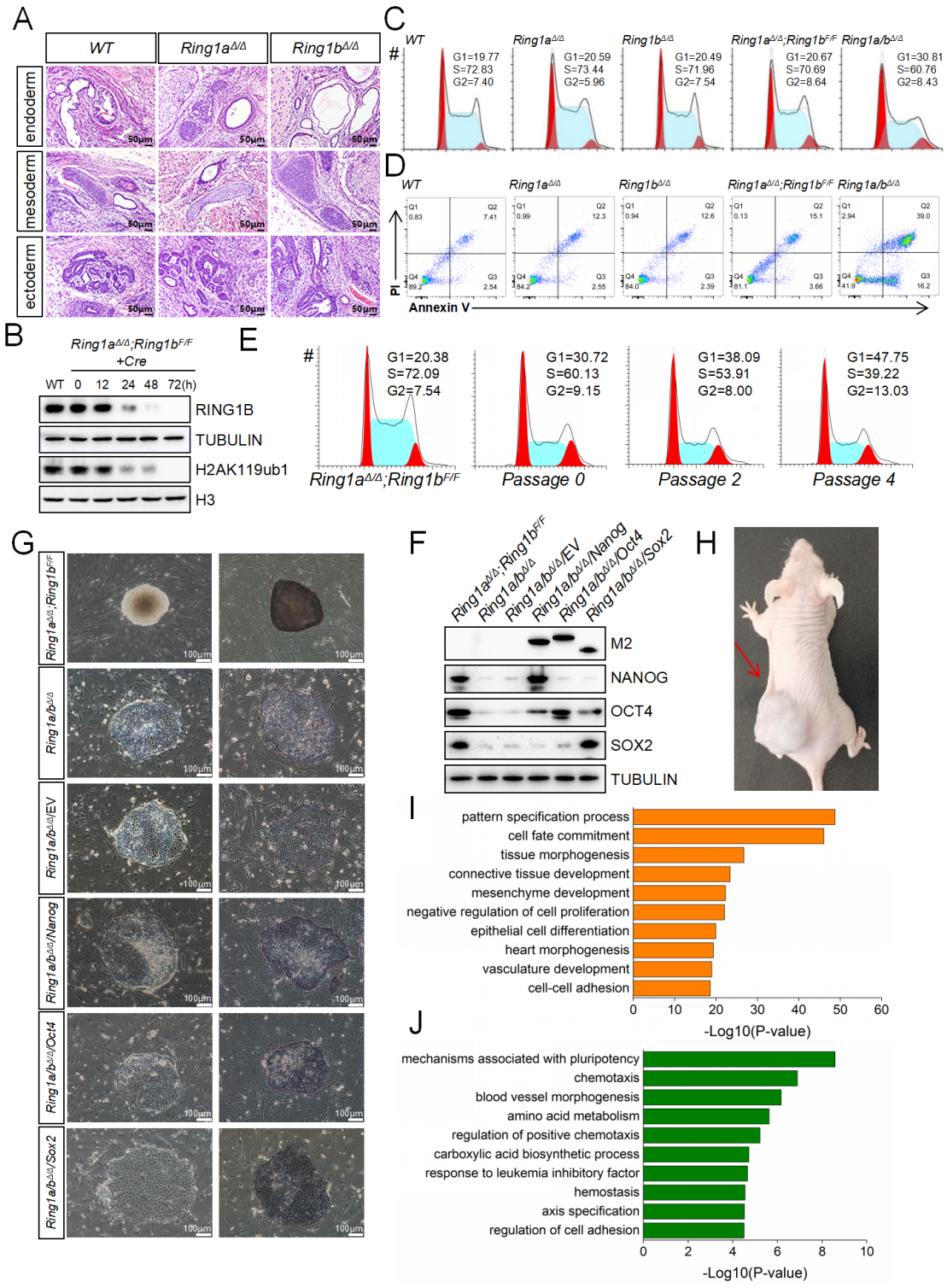

Figure S2. *Ring1a/b* play redundant and crucial roles in ESC self-renewal and maintenance. Related to Figure 3. (**A**) Representative images showing H&E staining of histological sections derived from teratomas generated from ESCs of the indicated genotypes. Shown is a representative of three injected mice. Scale bars, 50 μm. (**B**) Western blot showing RING1B and H2AK119ub1 levels in *Ring1a*$^{\Delta/\Delta}$*;Ring1b*$^{F/F}$ ESCs-transfected Cre recombinase for different time points. (**C**) Detection of changes in cell-cycle profile changes in cell-cycle profile determined by PI staining and FACS analysis. (**D**) Determination of apoptosis by flow cytometry of Annexin V/PI staining in ESCs of indicated genotypes. The percentages of Annexin V–positive (apoptotic) cells are within the two right quadrants. (**E**) Detection of changes in cell-cycle profile in *Ring1a*$^{\Delta/\Delta}$*;Ring1b*$^{F/F}$ following lenti-Cre infection determined by PI staining and FACS analysis. (**F**) Western blot demonstrating the levels of pluripotency factors in ESCs of indicated genotypes. The expression levels of the indicated FLAG-tagged proteins were detected with anti-Flag M2 antibody. Tubulin acted as a loading control. (**G**) Phase-contrast images of ESC colonies of indicated genotypes on MEF feeders (left). Representative images of AP staining of ESC colonies of indicated genotypes (right). (**H**) Representative images of mice bearing teratomas 28d after the injection of *Ring1a*$^{\Delta/\Delta}$*;Ring1b*$^{F/F}$ (left side, indicated by a red arrow) or *Ring1a/b*$^{\Delta/\Delta}$ ESCs (right side). Four mice were injected per condition. (**I and J**) Gene ontology analysis of overlapping genes up-regulated (**I**) and down-regulated (**J**) in *Ring1a*$^{\Delta/\Delta}$, *Ring1b*$^{\Delta/\Delta}$, and *Ring1a/b*$^{\Delta/\Delta}$ ESCs.

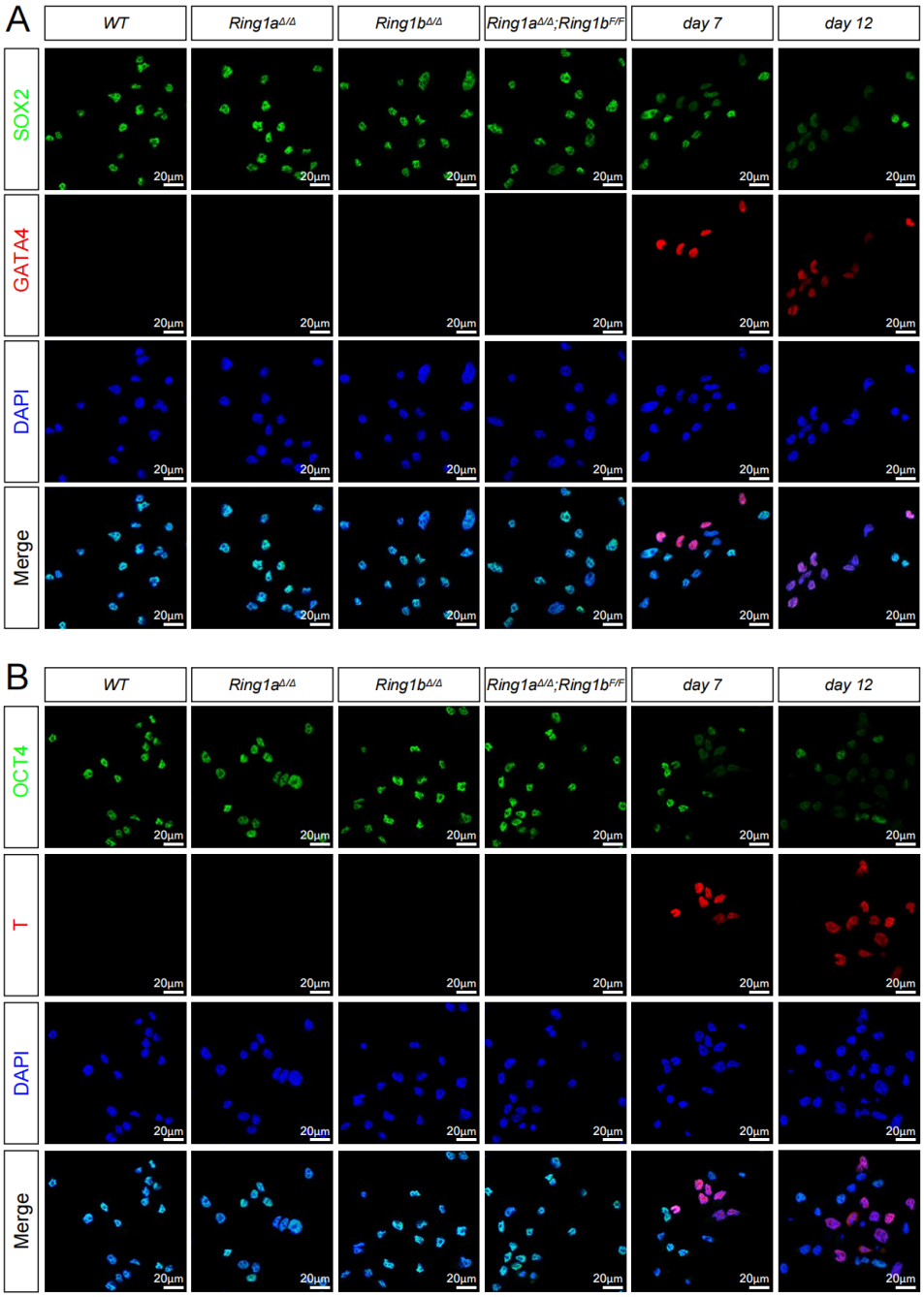

Figure S3. Combined *Ring1a/b* depletion triggers activation of lineage-specific genes and results in exit from ESC pluripotency. Related to Figure 3. IF analysis for SOX2, OCT4 (green), GATA4, T (red) or DAPI (blue) in *Ring1a*$^{\Delta/\Delta}$, *Ring1b*$^{\Delta/\Delta}$, and *Ring1a*$^{\Delta/\Delta}$*;Ring1b*$^{F/F}$ ESCs following lenti-Cre infection. Pictures were taken at 63x magnification using confocal microscopy. Merge, merged images.

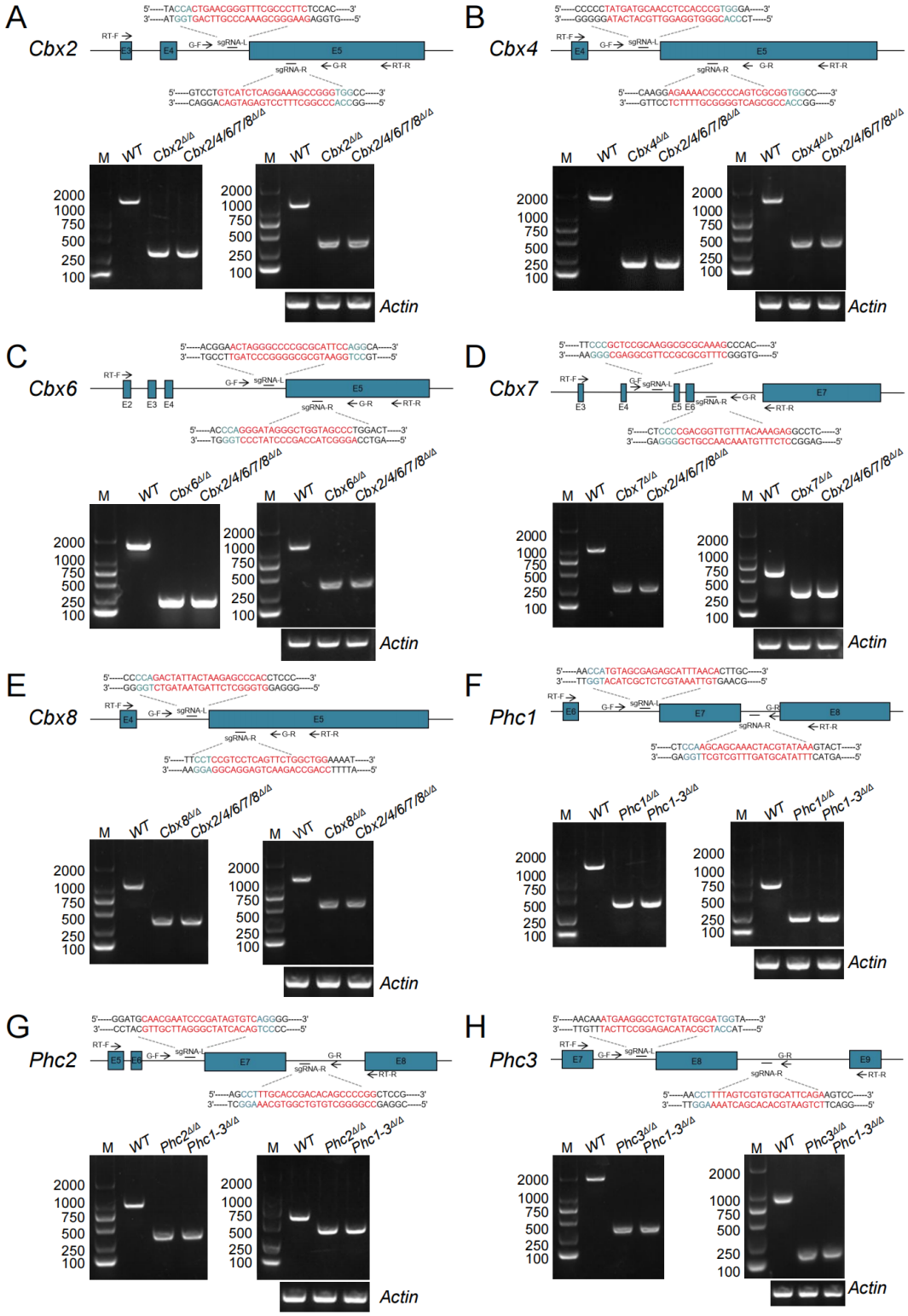

Figure S4. Generation of single and combined knockout ESC lines of *Cbx2/4/6/7/8* and *Phc1-3*. Related to Figure 4. (**A** to **H**) Top, schematic representation of CRISPR/Cas9 mediated knockout approaches to generate ESCs deficient in *Cbx2/4/6/7/8* and *Phc1-3*. PAM sequences are in blue following the sgRNA sequence highlighted in red. The locations of genomic PCR primers (G-F, Forward; G-R, Reverse) and RT-PCR primers (RT-F, Forward; RT-R, Reverse) are shown. Bottom, genotyping of ESCs

with indicated gene deletions using primers located upstream and downstream of the deleted region (left); RT-PCR analysis for residual mRNA revealed a shorter band in the mutants (right). *β-Actin* acted as a loading control.

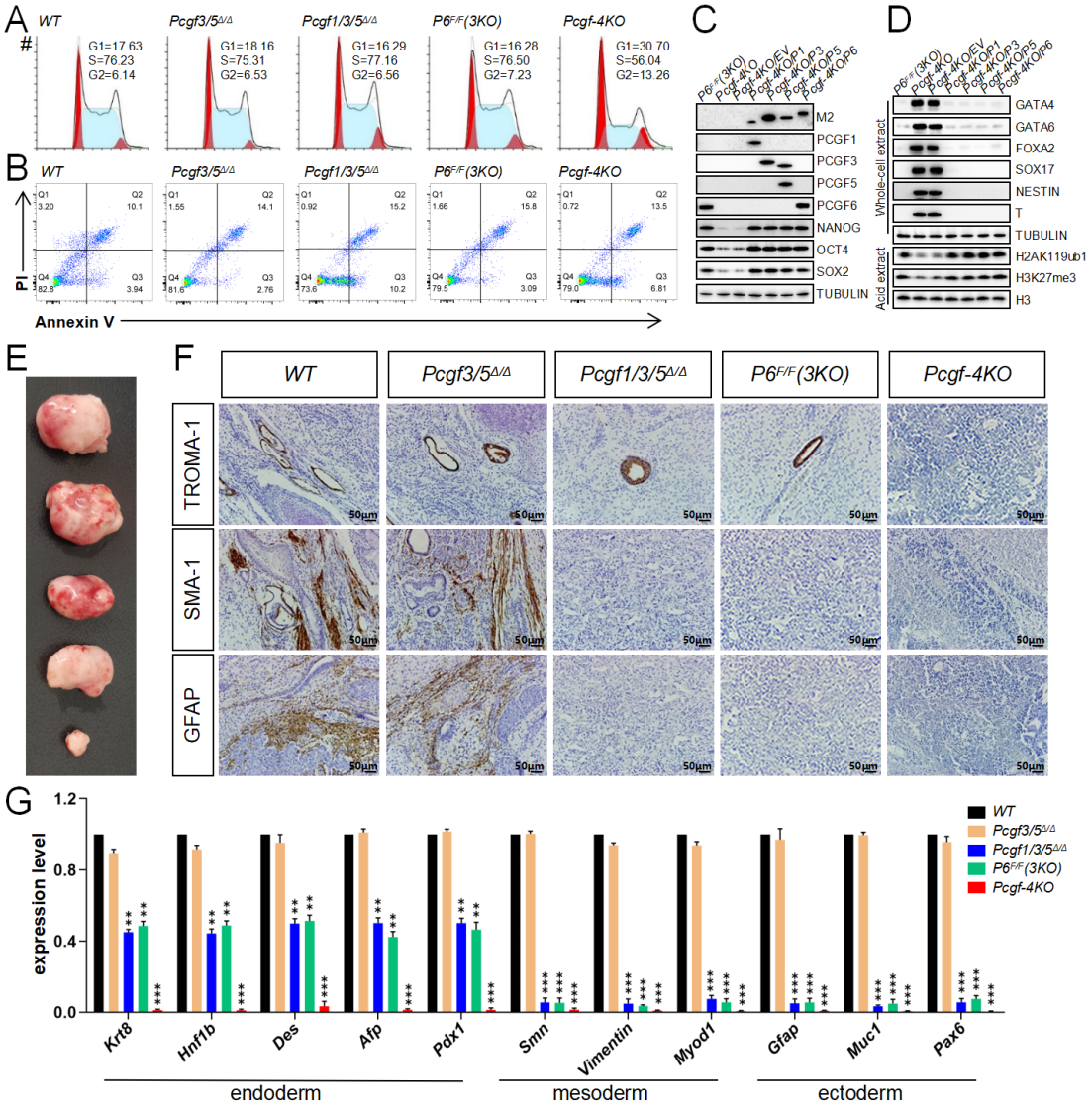

Figure S5. Disruption of ncPRC1 leads to profound differentiation defects in ESCs. Related to Figure 5. (**A**) Representative cell cycle profiles determined by PI-staining and FACS analysis. (**B**) Flow cytometric quantification of apoptosis with Annexin-V and PI. The percentages of Annexin V–positive (apoptotic) cells are within the two right quadrants. (**C** and **D**) Western blot demonstrating changes in the levels of selected PcG proteins, pluripotency factors, (**D**) germ layer markers and histone modifications, in ESCs of indicated genotypes. The expression levels of the indicated FLAG-tagged proteins were detected with anti-Flag M2 antibody. TUBULIN and H3 were used as loading controls. (**E**) Teratoma formation in immunodeficiency mice by *WT*, *Pcgf3/5*$^{\Delta/\Delta}$, *Pcgf1/3/5*$^{\Delta/\Delta}$, *Pcgf1/3/5*$^{\Delta/\Delta}$*;Pcgf6*$^{F/F}$ and *Pcgf1/3/5/6*$^{\Delta/\Delta}$ ESCs (from top to bottom) 28d after injection. (n=3 animals for each condition). (**F**) Immunohistochemical analysis of teratomas corresponding to the indicated genotypes using markers for endoderm (TROMA1) (top), mesoderm (smooth muscle actin 1 [SMA1]) (middle) and ectoderm (GFAP) (bottom). The scale bar is 50μm. (**G**) RT-qPCR analysis of the three germ layer markers in indicated

teratomas. Each value was normalized to its corresponding *actin* value and the expression level in WT ESCs was arbitrarily set to 1. Data are shown as the means ± SD for triplicate analysis. *p < 0.05, **p < 0.01, ***p < 0.001 (Student's t test) compared with the control.

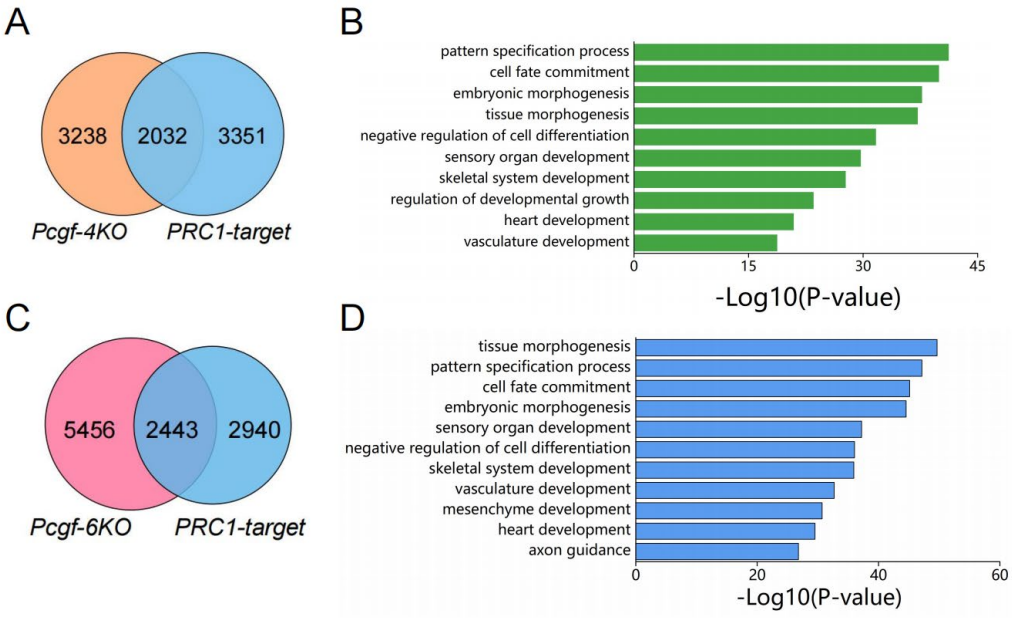

Figure S6. *Pcgf* shares target genes with PRC1, Related to Figure 7. (**A and C**) Venn diagram showing the overlap between genes differentially expressed after *Pcgf* deletion and those occupied by PRC1. (**B and D**) GO analysis for biological processes associated with the overlapping genes.

Table S1. Genes that are differentially expressed in *Ring1a*$^{\Delta/\Delta}$ vs. control ESCs.
Table S2. Genes that are differentially expressed in *Ring1b*$^{\Delta/\Delta}$ vs. control ESCs.
Table S3. Genes that are differentially expressed in *Ring1a/b*$^{\Delta/\Delta}$ vs. control ESCs.
Table S4. Genes that are differentially expressed in *Pcgf1/3/5/6*$^{\Delta/\Delta}$ vs. control ESCs.
Table S5. Genes that are differentially expressed in *Pcgf1/2/3/4/5/6*$^{\Delta/\Delta}$ vs. control ESCs.

Table S6: Cell lines used in this study

Cell Lines	Source（Original Validation）
Ezh1$^{\Delta/\Delta}$	(Huang et al., 2021) （Figure S5）
Ezh2$^{\Delta/\Delta}$	(Huang et al., 2021)（Figure S5）
Suz12$^{\Delta/\Delta}$	(Huang et al., 2021)（Figure S5）
Eed$^{\Delta/\Delta}$	(Huang et al., 2021)（Figure S5）
Jarid2$^{\Delta/\Delta}$	(Huang et al., 2021)（Figure S6）
Aebp2$^{\Delta/\Delta}$	(Huang et al., 2021)（Figure S6）
Phf1$^{\Delta/\Delta}$	(Huang et al., 2021)（Figure S6）
Mtf2$^{\Delta/\Delta}$	(Huang et al., 2021)（Figure S6）
Phf19$^{\Delta/\Delta}$	(Huang et al., 2021)（Figure S6）
Pcgf1$^{\Delta/\Delta}$	this study
Pcgf2$^{\Delta/\Delta}$	this study
Pcgf3$^{\Delta/\Delta}$	this study
Pcgf4$^{\Delta/\Delta}$	this study
Pcgf5$^{\Delta/\Delta}$	this study
Pcgf6$^{\Delta/\Delta}$	this study
Bcor$^{\Delta/\Delta}$	(Qin et al., 2021)（Figure S1）
Bcorl1$^{\Delta/\Delta}$	(Qin et al., 2021)（Figure S1）
Skp1$^{\Delta/\Delta}$	(Qin et al., 2021)（Figure S1）
Cbx2$^{\Delta/\Delta}$	This study
Cbx4$^{\Delta/\Delta}$	This study
Cbx6$^{\Delta/\Delta}$	This study
Cbx7$^{\Delta/\Delta}$	This study
Cbx8$^{\Delta/\Delta}$	This study
Hp1γ$^{\Delta/\Delta}$	(Qin et al., 2021)（Figure S1）
Hdac1$^{\Delta/\Delta}$	(Qin et al., 2021)（Figure S1）
Hdac2$^{\Delta/\Delta}$	(Qin et al., 2021)（Figure S1）
E2f6$^{\Delta/\Delta}$	(Qin et al., 2021)（Figure S1）
G9a$^{\Delta/\Delta}$	(Qin et al., 2021)（Figure S1）
Glp$^{\Delta/\Delta}$	(Qin et al., 2021)（Figure S1）
Rybp$^{\Delta/\Delta}$	(Zhao et al., 2018)（Figure S3）
Yaf2$^{\Delta/\Delta}$	(Zhao et al., 2018)（Figure S1）
Ring1a$^{\Delta/\Delta}$	This study
Ring1b$^{\Delta/\Delta}$	This study

Usp7$^{\Delta/\Delta}$	(Qin et al., 2021)（Figure S1）
Kdm2b$^{\Delta/\Delta}$	(Qin et al., 2021)（Figure S1）
Scmh1$^{\Delta/\Delta}$	(Qin et al., 2021)（Figure S1）
Scml2$^{\Delta/\Delta}$	(Qin et al., 2021)（Figure S1）
Phc1$^{\Delta/\Delta}$	This study
Phc2$^{\Delta/\Delta}$	This study
Phc3$^{\Delta/\Delta}$	This study
Ck2α1$^{\Delta/\Delta}$	(Qin et al., 2021)（Figure S1）
Ck2α2$^{\Delta/\Delta}$	(Qin et al., 2021)（Figure S1）
Ck2b$^{\Delta/\Delta}$	(Qin et al., 2021)（Figure S1）
Auts2$^{\Delta/\Delta}$	(Qin et al., 2021)（Figure S1）
Fbrs$^{\Delta/\Delta}$	(Qin et al., 2021)（Figure S1）
Fbrsl1$^{\Delta/\Delta}$	(Qin et al., 2021)（Figure S1）
Mga$^{\Delta/\Delta}$	(Qin et al., 2021)（Figure S1）
Max$^{\Delta/\Delta}$	(Qin et al., 2021)（Figure S1）
Dp-1$^{\Delta/\Delta}$	(Qin et al., 2021)（Figure S1）
Wdr5$^{\Delta/\Delta}$	(Qin et al., 2021) (Figure S1）
L3mbtl2$^{\Delta/\Delta}$	(Huang et al., 2018)（Figure S2）
Cbx2/4/6/7/8$^{\Delta/\Delta}$	this study
Rybp/Yaf2$^{\Delta/\Delta}$	(Zhao et al., 2018)（Figure S1 and S3）
Phc1/2/3$^{\Delta/\Delta}$	this study
Ring1a$^{\Delta/\Delta}$*;Ring1b*$^{F/F}$	this study
Ring1a/b$^{\Delta/\Delta}$	this study
Pcgf3/5$^{\Delta/\Delta}$	this study
Pcgf2/4$^{\Delta/\Delta}$	this study
Pcgf1/3/5$^{\Delta/\Delta}$	this study
Pcgf1/3/5$^{\Delta/\Delta}$*;Pcgf6*$^{F/F}$	this study
Pcgf1/3/5/6$^{\Delta/\Delta}$	this study
Pcgf1/2/3/4/5$^{\Delta/\Delta}$	this study
Pcgf1/2/3/4/5$^{\Delta/\Delta}$*;Pcgf6*$^{F/F}$	this study
Pcgf1/2/3/4/5/6$^{\Delta/\Delta}$	this study

Table S7: Summary of the primers used in this study

Gene Name	Forward Primer	Reverse Primer	Application
Cbx2	CTAATCTCCCTCCCGGTTCC	GGGGAGGGAGCTGTATCAGT	Genomic-PCR
Cbx4	CACGAGCCCTTCCCTAAACAT	TCCTATAGGGAAGGGGACGTG	Genomic-PCR
Cbx6	CACACACGATGACTTAGGGGT	ATGGCGAGATAGCACCGAGA	Genomic-PCR
Cbx7	CCAAGGGCAATGAGAAGCTC	CCACGGATCAGCCTCTGAAA	Genomic-PCR
Cbx8	AGGACTTAGCTGCACCAGAA	CTCCACACACCCTCCAAAATCC	Genomic-PCR
Phc1	TTTGGTTCTGTGGCTTTGGT	ACAAGGCAAGCACACACAAA	Genomic-PCR
Phc2	AGCTAGGTTATGAGTCCGGC	GTCACCCTCCTTTACCTCCC	Genomic-PCR

Phc3	ACACTTACTTGGGAAGCTTTCT	CTTTTAACTGAGAACTAAT	Genomic-PCR
Cbx2	GAACATTTTGGACCCGAGGC	ACCTCACAGTAGTTGGCCAG	RT-PCR
Cbx4	TGAAATGGAGAGGCTGGTCC	TCCTATAGGGAAGGGGACGTG	RT-PCR
Cbx6	AGGAAAGGGAACGTGAGCTG	CCAAACACTGCACACAGAGC	RT-PCR
Cbx7	GGAGCACATCTTGGACCCT	GTTGTCCTGATCCTGTCCCC	RT-PCR
Cbx8	AAAGGGAACGGGAGATGGAG	TCCCCTACCAAACCACAGTC	RT-PCR
Phc1	AGTCTCCTGGAGTTCATGCA	TGTTGGAACTGTTGCTGGTG	RT-PCR
Phc2	AGCCAAGCACAGATGTACCT	CTTGTGGACATGCGTGGTAG	RT-PCR
Phc3	CACTCGGACATCAAGCATCC	CATCCTTGCACACTCATCGG	RT-PCR
Afp	TATGGACTCTCAGGCTGCTG	GCCCTGTTTTCTTCATGTGC	RT-PCR
Sox7	GACCCTGGCTTCCTCCTC	GAGTACTCACCCCTGTCCTC	RT-PCR
Gata4	TCTCTTTCCCGGGGACTACT	GGTAGGGGCTGGAGTAGGAG	RT-PCR
Hnf1b	CTTGGAGGAGTTACTGCCGT	CGTGGCCATTGGTGAGAGTA	RT-PCR
Gata6	CTCTGCACGCTTTCCCTACT	GTAGGTCGGGTGATGGTGAT	RT-PCR
Foxa2	GACATACCGACGCAGCTACA	GGCACCTTGAGAAAGCAGTC	RT-PCR
Otx1	CGGAAGCTATGGTCAGGGAT	TGAAGATTGGCTCAGTGGGT	RT-PCR
Meis	GTTCACCACCTAAACCACGG	CGTTGACAGCAGATCCCATG	RT-PCR
Lhx5	ACCTCAACTGCTTCACCTGT	AGTAGTCGTCCTTGCACACA	RT-PCR
Nestin	CAACCTTGCCGAAGAGCTG	GCATTCTTCTCCGCCTCGA	RT-PCR
Krt18	GACCATGCAAGACCTGAACG	GCCCCTTCTTCTCCAGATGT	RT-PCR
Bmp4	TCTTTACCGGCTCCAGTCTG	AACTCCTCACAGTGTTGGCT	RT-PCR
Eomes	AAGCGTCCAAGAAGTTTCCG	GTCCGCGTCACTGAGCAT	RT-PCR
Bmp6	CTCTTCTTCGGGCTTCCTCT	CTGAGGCTGCTGGAGACC	RT-PCR
Msx2	CGCTCATGTCCGACAAGAAG	ATTTTCCGACTTGACCGAGG	RT-PCR
T	TCCCGGTGCTGAAGGTAAAT	CCCACTCCCCGTTCACATAT	RT-PCR
Hand1	GAGCGGCCTTACTTCCAGA	GGTCCTGAGCCTTTTCGTTT	RT-PCR
Tead4	TGCAGAGGGTGTATGGAGC	ATCTTGCCTTCCTCCGTCAG	RT-PCR
zeb1	AGCTGACTGTGAAGGTGGC	CGTTGTCTTGCCAGCAGTT	RT-PCR
Actin	AGCCATGTACGTAGCCATCC	CTCTCAGCTGTGGTGGTGAA	RT-PCR
Vim	GCTTCAAGACTCGGTGGACT	TTTTGTTCTGCTGCTCGAGG	RT-PCR
Ema	GCATTCGGGCTCCTTTCTTC	TCTGAGTTGCTGCTGTGGA	RT-PCR
Des	CCAGGCCTACTCGTCCAG	GCGGGATGTCATTGAACTCG	RT-PCR
Pdx1	ACACAGCTCTACAAGGACCC	ACTTCCCTGCTCCAGTGATC	RT-PCR
Myod1	TCCGGGACATAGACTTGACAG	TGCTCCTCCGGTTTCAGG	RT-PCR
Pax6	TCTGCAGGTATCCAACGGTT	GCAAAGATGGAAGGGCACTC	RT-PCR
Krt8	GTGAACCAGAGCCTGTTGAG	CATCTTGTTCTGCTGCTCCA	RT-PCR
Smn	CCGGCCAGAGTGATGATTCT	GCAGGTTTTCTTCTGGCTGT	RT-PCR
Gfap	ACGCTTCTCCTTGTCTCGAA	CGGACCTTCTCGATGTAGCT	RT-PCR
Pcgf1	CTGTGTGAACCCAAACGAAGG	GTCATGTGATCTGGGAGAACCT	Genomic-PCR
Pcgf2	CCACCCTGGCTCATAGAGAT	AGGAAGAGGCCAGCAGTAAG	Genomic-PCR
Pcgf3	GCTCTTGCCCCTTAGTGACT	TCTAAGCACAGTGACAGCCA	Genomic-PCR
Pcgf4	CTGTTACATGAAAGGCCTACCT	TCTGTCGTCAAGATCTAACCCA	Genomic-PCR
Pcgf5	GGTAACTGCTGCTTTGTCCC	AATCTCCTTCTGGCAGCAGA	Genomic-PCR

Pcgf6	F: ATTTAGGGCACTCTGGGTCC	R1: AACCCTCTCAACATCCTGCA	Genomic-PCR
		R2: CCTCCTCCCCACTCTCTTTC	Genomic-PCR
Ring1a	CCAGCCCTAGTCCTCTCAAC	TAGTCTTCACGTACCTGGGG	Genomic-PCR
Ring1b	F: AGGGCTACACAGAGAAACCG	R1: TACACCCCTCCAGTCTTCAG	Genomic-PCR
		R2: TCACTTGTGAGGGTAGGGG	Genomic-PCR
Pcgf1	CGATGAGGCTTCGGAACCAG	AAAGGAGATGGCTTGCCGAA	RT-PCR
Pcgf2	AAATCACGGAGCTGAACCCT	GGGGAAGTAGGATGGGTAGC	RT-PCR
Pcgf3	ATTGACGCAACCACAGTGAC	CTTGAGAGTGTGGTCCTTGC	RT-PCR
Pcgf4	CGCTTGGCTCGCATTCATTT	GGCAATGTCCATTAGCGTGT	RT-PCR
Pcgf5	ATCTGATCAAGCCCACGACA	CTGTGCAATCTGTCGACGAG	RT-PCR
Pcgf6	GGAGGAGGAAGAGATGAGCC	GTGACAACAGAAGCCAGCTC	RT-PCR
Ring1a	CAGCAAAACGTGGGAACTGA	GCTCTGTGGTTTCCTGCTG	RT-PCR
Ring1b	GCTGGGATGTGGCTATGACA	GCCCAGAGTCATCAGAGGTT	RT-PCR

Table S8. Additional datasets used in this study, related to Figures 2 and 3.

CHIP-Seq		
Name	**Source**	**Identifier**
PCGF1	(Scelfo et al., 2019)	GSE122715
PCGF2	(Scelfo et al., 2019)	GSE122715
PCGF3	(Scelfo et al., 2019)	GSE122715
PCGF5	(Yao et al., 2018)	GSE107377
PCGF6	(Scelfo et al., 2019)	GSE122715
RING1B	(Scelfo et al., 2019)	GSE122715
	(Jaensch et al., 2021)	GSE151899
H2AK119ub1	(Scelfo et al., 2019)	GSE122715
RNA-Seq		
Gene Name	**Source**	**Identifier**
Pcgf2/4-dKO	(Scelfo et al., 2019)	GSE122715

Supplemental Experimental Procedures

Cell culture

ESCs were cultured on gelatinized plates or on mitomycin-treated feeder MEFs in DMEM high glucose (Gibco), which was supplemented with 15% fetal calf serum (Gibco), penicillin-streptomycin (Gibco), 1000U/mL of LIF (Leukaemia inhibitory factor), L-Glutamine (Gibco), non-essential amino acids (Gibco) and β-mercaptoethanol (Sigma).

Colony formation and alkaline phosphatase staining

Resuspended single ESCs were planted on feeder MEFs at an appropriate density for 7-10 days to form colonies, which were washed with PBS twice and fixed with 4% paraformaldehyde (PFA) briefly, and then incubated with staining solution for 15 min at room temperature in dark. Finally, the stained colonies were photographed microscopically.

Teratoma, HE staining and immunohistochemistry

Teratoma formation assay was performed as described(Qin et al., 2021). 10^6 ESCs were trypsinized and resuspended in PBS, which were injected subcutaneously into 8-week-old immunodeficient mice. After 4 weeks, teratomas were fixed with 4% phosphate-buffered formaldehyde at 4°C overnight, and then paraffin-embedded tissue was sliced and stained with hematoxylin and eosin. For immunohistochemistry, paraffin sections were incubated with TROMA-1(markers for endoderm), SMA (markers for mesoderm) and GFAP (markers for ectoderm) respectively and then photographed by BX53 semi-electric fluorescence microscope (Olympus). The experimental animal facility has been accredited by the Association for Assessment and Accreditation of Laboratory Animal Care International, and all the animal work was performed with the approval of the Institutional Animal Care and Use Committee of the Model Animal Research Center of Nanjing University.

Histone extraction and Western blot

Histone extraction was performed as described previously(Qin et al., 2012). Briefly, ESCs were washed with ice-cold PBS, resuspended in Triton extraction buffer (TEB: PBS containing 0.5% Triton X-100 (v/v), 2 mM phenylmethylsulfonyl fluoride (PMSF), 0.02% (w/v) NaN3) and then centrifuged. The nuclear pellet was resuspended in 200 μL 0.2N HCl at 4°C overnight. The supernatants were separated via SDS-PAGE and analyzed by immunoblotting. For whole cell lysates, cells were lysed in RIPA buffer (50 mM Tris pH 8.0, 150 mM NaCl, 5 mM EDTA, and protease inhibitors) on ice, and centrifuged to collect the supernatant for the analysis.

RNA preparation and analysis

RNA was extracted from ESCs with Trizol reagent (Thermo Fisher Scientific) according to the standard protocol. The first strand cDNA was synthesized by HiScript 1st Strand cDNA Synthesis Kit (Vazyme) from total RNA (2.5μg) following the manufacturer's instructions. Gene expression was quantified by RT-qPCR with PowerUp™ SYBR® Green Master Mix (Vazyme) on StepOnePlus™ Real-Time PCR System. The expression of indicated genes was normalized to the content of *β-Actin* mRNA. Primer details are given in table S7 and in a previous report(Qin et al., 2021).

RNA-seq analysis

Total RNA was isolated with Trizol reagent (Invitrogen) from the indicated cell lines according to the manufacturer's instructions, then high-quality RNA sample was quantified with a NanoDrop-1000 spectrophotometer (NanoDrop Technologies) and sequenced by Shanghai Majorbio Bio-pharm Biotechnology Co., Ltd (Shanghai, China). Briefly, RNA-seq transcriptome library was constructed with TruSeq™ RNA sample preparation kit from

Illumina (San Diego, CA), and subsequently, the library was sequenced with Illumina HiSeq 4000. The sequencing data was mapped to mouse genome (Ensemble GRCm38.p5) with orientation mode by TopHat (version2.1.1). For data analysis, the expression of each gene was calculated by FPKM (fragments per kilobase of transcript per million fragments mapped) method. Quantitative analysis of gene abundance and differential expression was performed by RSEM and R statistical package software EdgeR (Empirical analysis of Digital Gene Expression in R). RNA-seq data in this study have been deposited to the Gene Expression Omnibus.

Lentiviral production and infection

Lentiviral supernatants were prepared as described(Qin et al., 2012). Briefly, lentivirus was prepared in HEK293T cells that were cotransfected with the respective lentiviral expression vectors, and a mixture of the packaging plasmids. Virus-containing supernatant was collected at 48h and 72h after transfection, pooled together, passed through a 0.45-μm filter and concentrated by ultra-centrifugation at 4°C. ESCs were infected by the virus particles with Polybrene (Sigma, 8μg/mL). After 24h, the infected cells were selected with puromycin (2 μg/mL) for 1 week and single colonies were picked up and further cultured.

Flow cytometry

ESCs were harvested by trypsin and washed twice with cold PBS. For apoptosis analysis, the cells were stained with fluorescein isothiocyanate-Annexin V (BD Pharmingen) and/or PI for 30 min in dark. For cell cycle analysis, ESCs were fixed with 70% ethanol at -20°C overnight, incubated with RNase A (200g/mL) for 30 min at 37°C subsequently after being washed with PBS, and then stained with PI for 30 min in dark for the analysis by a LSRFortessa flow cytometer equipped with Cell Quest software (BD Biosciences).

Immunofluorescence

ESCs were cultured on gelatin-coated glass coverslips, and then standard immunofluorescence staining protocol was performed. Briefly, ESCs were fixed in 4% (w/v) paraformaldehyde for 15 min at room temperature and rinsed in PBS, and then permeabilised in 0.5% Triton X-100 in PBS for 20 min. After three times washes with PBS, cells were incubated with blocking buffer (PBS, 10% (v/v) goat serum, 1% (w/v) BSA) for 30 min subsequently, to block nonspecific binding sites. After that, ESCs were incubated sequentially with the appropriate dilutions of primary antibody solution at 4°C overnight. Then ESCs were washed with PBS, followed by incubating with fluorophores-conjugated (Alexa Flour 488 or 594 dyes) secondary antibody for 1h in dark. Finally, the cells were counterstained with DAPI (4′,6-diamino-2-phenylindole) in BSA for 5 min for DNA staining. Fluorescent images were taken by Zeiss LSM 880 laser scanning confocal microscope at 63× magnification.

Supplementary References

Huang, Y., Su, T., Wang, C., Dong, L., Liu, S., Zhu, Y., Hao, K., Xia, Y., Jiang, Q., and Qin, J. (2021). Rbbp4 Suppresses Premature Differentiation of Embryonic Stem Cells. Stem cell reports *16*, 566-581.

Huang, Y., Zhao, W., Wang, C., Zhu, Y., Liu, M., Tong, H., Xia, Y., Jiang, Q., and Qin, J. (2018). Combinatorial

Control of Recruitment of a Variant PRC1.6 Complex in Embryonic Stem Cells. Cell reports *22*, 3032-3043.

Jaensch, E.S., Zhu, J., Cochrane, J.C., Marr, S.K., Oei, T.A., Damle, M., McCaslin, E.Z., and Kingston, R.E. (2021). A Polycomb domain found in committed cells impairs differentiation when introduced into PRC1 in pluripotent cells. Molecular cell *81*, 4677-4691.e4678.

Qin, J., Wang, C., Zhu, Y., Su, T., Dong, L., Huang, Y., and Hao, K. (2021). Mga safeguards embryonic stem cells from acquiring extraembryonic endoderm fates. Science advances *7*.

Qin, J., Whyte, W.A., Anderssen, E., Apostolou, E., Chen, H.H., Akbarian, S., Bronson, R.T., Hochedlinger, K., Ramaswamy, S., Young, R.A*., et al.* (2012). The polycomb group protein L3mbtl2 assembles an atypical PRC1-family complex that is essential in pluripotent stem cells and early development. Cell stem cell *11*, 319-332.

Scelfo, A., Fernández-Pérez, D., Tamburri, S., Zanotti, M., Lavarone, E., Soldi, M., Bonaldi, T., Ferrari, K.J., and Pasini, D. (2019). Functional Landscape of PCGF Proteins Reveals Both RING1A/B-Dependent-and RING1A/B-Independent-Specific Activities. Molecular cell *74*, 1037-1052.e1037.

Yao, M., Zhou, X., Zhou, J., Gong, S., Hu, G., Li, J., Huang, K., Lai, P., Shi, G., Hutchins, A.P*., et al.* (2018). PCGF5 is required for neural differentiation of embryonic stem cells. Nature communications *9*, 1463.

Zhao, W., Liu, M., Ji, H., Zhu, Y., Wang, C., Huang, Y., Ma, X., Xing, G., Xia, Y., Jiang, Q*., et al.* (2018). The polycomb group protein Yaf2 regulates the pluripotency of embryonic stem cells in a phosphorylation-dependent manner. The Journal of biological chemistry *293*, 12793-12804.